8/3/06 9:14 AM LA-UR-06-5184
DT# 48430 QA: NA ab 8/22/06

Eruptive and geomorphic processes at the Lathrop Wells scoria cone volcano

Greg A. Valentine[a], Donathan J. Krier, Frank V. Perry, Grant Heiken[b]

Mail Stop D462, Earth and Environmental Sciences Division, Los Alamos National Laboratory, Los Alamos, NM 87545 USA

[a]*email: gav@lanl.gov*

[b]*current address: 331 Windantide Place, Freeland, WA 98249-9683*

Abstract

The ~80 ka Lathrop Wells volcano (southern Nevada, U.S.A.) preserves evidence for a range of explosive processes and emplacement mechanisms of pyroclastic deposits and lava fields in a small-volume basaltic center. Early cone building by Strombolian bursts was accompanied by development of a fan-like lava field reaching ~800 m distance from the cone, built upon a gently sloping surface. Lava flows carried rafts of cone deposits, which provide indirect evidence for cone facies in lieu of direct exposures in the active quarry. Subsequent activity was of a violent Strombolian nature, with many episodes of sustained eruption columns up to a few km in height. These deposited layers of scoria lapilli and ash in different directions depending upon wind direction at the time of a given episode, reaching up to ~20 km from the vent, and also produced the bulk of the scoria cone. Lava effusion migrated from south to north around the eastern base of the cone as accumulation of lavas successively reversed the topography at the base of the cone. Late lavas were emplaced during violent Strombolian activity and continued for some time after explosive eruptions had waned. Volumes of the eruptive products are: fallout – 0.07 km^3, scoria cone – 0.02 km^3, and lavas – 0.03 km^3. Shallow-derived xenolith concentrations

suggest an upper bound on average conduit diameter of ~21 m in the uppermost 335 m beneath the volcano. The volcano was constructed over a period of at least seven months with cone building occurring only during part of that time, based upon analogy with historical eruptions. Post-eruptive geomorphic evolution varied for the three main surface types that were produced by volcanic activity: (1) scoria cone, (2) low relief surfaces (including lavas) with abundant pyroclastic material, and (3) lavas with little pyroclastic material. The role of these different initial textures must be accounted for in estimating relative ages of volcanic surfaces, and failure to account for this resulted in previous erroneous interpretation that the volcano is polycyclic (eruptions separated by 1,000s-10,000s of years). Lathrop Wells volcano provides an example of the wide range of eruptive processes that can occur with little change in major element composition; the variation in explosive and effusive processes, including their simultaneous occurrence, must result entirely from fluid dynamic, crystallization, and degassing processes in the ascending multiphase magma. The volcano also provides key analog information regarding processes that are important for volcanic risk assessment at the proposed Yucca Mountain radioactive waste repository, ~ 18 km north of the volcano.

Keywords: scoria cone, lava, fallout deposit, Strombolian, violent Strombolian, geomorphology

1. Introduction

Lathrop Wells volcano is the youngest of eight small-volume, trachybasaltic Quaternary volcanoes in the Southwestern Nevada Volcanic Field (Fleck et al., 1996; Perry et al., 1998; Valentine and Perry, 2006). It is located 18 km south of the U.S. Department of Energy's proposed repository for high-level nuclear waste and spent nuclear fuel at Yucca Mountain (Fig. 1). Because of its relatively young age (~75-80 ka; Heizler et al., 1999) and good state of

preservation, the volcano provides key information on the nature of a potential future volcanic event at Yucca Mountain (over periods of 10^4-10^6 years) that is used for repository risk assessments (Crowe, 1986; Crowe et al., 2006). In addition, Lathrop Wells volcano preserves much evidence for the complex and often overlooked range of processes that accompany formation and geomorphic evolution of small scoria-cone volcanoes that are the most abundant type of continental volcanic landform (Wood, 1980a).

In addition to outcrops and excavated pits for fallout characterization, commercial quarrying of the Lathrop Wells cone over the last 15 years has exposed sequential views of the internal structure that provide clues to the sequence of eruptive processes. Activity began with initial Strombolian eruptions accompanied by lava effusion onto a gently sloping alluvial plain. Pyroclastic activity evolved towards increasingly energetic violent Strombolian eruptions as time progressed, while lavas continued to effuse from the base of the growing cone. Three main types of volcanic surfaces were generated by the eruptive activity: (1) scoria cone, (2) surfaces with abundant pyroclastic material (either fallout or rafted cone material), and (3) lava surfaces with little pyroclastic material. After eruptions ceased, these three surface types evolved differently, while eolian and colluvial processes buried and preserved parts of the fallout deposit. We discuss the implications of our conclusions for emplacement mechanisms of volcanic products associated with scoria-cone eruptions and for geomorphic interpretations of different volcanic surfaces. With respect to the latter, the degree of cone or lava surface degradation is often used as an indicator of relative age (e.g., Wood 1980b; Hooper and Sheridan, 1998; Wells et al., 1985, 1990; Bradshaw and Smith, 1994). In an earlier paper (Valentine et al., 2006) we showed the importance of accounting for different initial characteristics of the volcanic surfaces in order to avoid erroneous interpretations of relative ages of lava fields associated with the ~1 Ma

volcanoes in Crater Flat. Previous geomorphic interpretations of Lathrop Wells as a polycyclic volcano (Wells et al., 1990) also failed to account for the different initial surface characteristics.

Our conclusions about Lathrop Wells volcano, along with other basaltic centers in the southern Nevada region, provide analog information for three main issues that are important in risk assessment for the proposed Yucca Mountain repository: (1) The nature of subsurface plumbing of a volcanic event were one to intersect the 250-350 m deep repository, namely the number and size of dikes and conduits that might transport radioactive waste to the surface (e.g., Crowe et al., 1983; Doubik and Hill, 1999; Woods et al., 2002; Dartevelle and Valentine, 2005). (2) Types of explosive activity that might disperse contaminants over distances of ~20 km or greater (e.g., Jarzemba, 1997; Keating et al., submitted). (3) The fate of contaminated pyroclastic deposits as they are exposed to post-eruptive geomorphic processes, which provides information for surface transport models (e.g., Pelletier et al., submitted).

Terminology in this paper follows that of Valentine et al. (2006, online data supplement 2006173 available at http://www.geosociety.org/pubs/ft2006.htm).

2. Geologic Setting

Volcanism in the Southwestern Nevada Volcanic Field began in the mid-Miocene with eruptions at several large calderas and silicic volcanic centers (Fig. 1; Sawyer et al., 1994). Silicic volcanism in the area around Yucca Mountain began to wane after ~11.45 Ma (with the eruption of the Ammonia Tanks Tuff), finally ending with eruptions that formed the Black Mountain caldera ~9.4 Ma (Sawyer et al., 1994). Waning silicic activity gave way to large basaltic centers, with volumes up to ~10 km^3, during late Miocene. Basaltic volcanism continued sporadically in the region, with a general decrease in volume per volcano, including the most recent eruption that produced the Lathrop Wells volcano at ~80 ka (Crowe, 1986; Fleck

et al., 1996; Perry et al., 1998; Heizler et al., 1999; Valentine and Perry, 2006).

Basin-and-Range faulting has produced a dominant N-S grain of normal faults that intersects the NW-SE trending Walker Lane shear zone along the southwestern margin of the volcanic field. Lathrop Wells volcano is located in the transition between dominantly N-S trending normal faults to the right-lateral shear of the Walker Lane. In detail, the volcano resides at the intersection of closely spaced splays of the northwest-trending Windy Wash and the northeast-trending Stagecoach Road normal fault systems that define the southern extent of narrow, linear ridges of Miocene-age ignimbrites of Yucca Mountain. Within these fault systems, the volcano is located on an eastward tilted fault block, between major west-dipping normal faults, that is partly covered by a thin veneer of alluvial fan deposits (Potter et al., 2002). Based upon these observations and those at other basaltic volcanoes in the region back to the Miocene (e.g., Valentine and Krogh, 2006), it seems likely that the dike system that fed Lathrop Wells eruptions occupied a normal fault at shallow depths.

3. Previous work

Lathrop Wells volcano was first evaluated from a nuclear waste disposal and risk-assessment perspective by Crowe and Carr (1980). Numerous other investigations (Vaniman and Crowe, 1981; Crowe et al., 1983, 1986; Crowe, 1986; Champion, 1991; Wells et al.,1990, 1991, 1992; Turin et al., 1991, 1992; Zreda et al., 1993; Perry et al., 1998; Valentine et al., 2005; Valentine and Harrington, 2006; Valentine et al., 2006) added geochronologic, petrologic, geomorphic, paleomagnetic, and volcanological data and interpretations for Lathrop Wells volcano and the several nearby scoria cones that together make up the Crater Flat volcanic zone (Crowe and Perry, 1989). Despite the numerous papers that touch upon the Lathrop Wells

volcano, the literature remains confused on several aspects of its eruption sequence and a clear understanding of that sequence has not emerged previously. For example, some workers refer to the entire sequence as a "Strombolian" sequence and infer the presence of multiple vents scattered throughout the lava fields (e.g., Perry et al., 1998) with eruptions potentially separated by substantial periods of time (although not explicitly stated, the time intervals implied by Wells et al., 1990, must be on the order of 10^3-10^4 years or more), while Wohletz (1986) infers the occurrence of a major hydrovolcanic explosion phase accompanied by formation of a tuff ring early in the eruptive sequence. After more than a decade of debate on the age of the Lathrop Wells event(s), including evidence from K-Ar dating, cosmogenic ^{3}He and ^{36}Cl exposure ages (Zreda et al., 1993), and paleomagnetic and geomorphic studies, Heizler et al. (1999) concluded that reproducible ^{40}Ar/^{39}Ar ages of 77.3 ± 6.0 ka and 76.6 ± 4.9 ka (2σ) for the early and late erupted lavas, respectively, represent the most probable age for the volcano. For simplicity we refer to the age as ~80 ka.

4. Overview of composition and eruptive sequence

Compositionally, Lathrop Wells is a trachybasalt (Table 1) with an Mg-number of ~54 that reflects substantial fractionation of the parent magma (Vaniman and Crowe, 1981; Crowe et al., 1995; Perry and Straub, 1996). Most of the volcanic products are sparsely porphyritic, with 1-4 vol% olivine phenocrysts and a groundmass dominated by plagioclase; however, two lobes of the early lava field and the lower cone deposits also contain 1-4 vol% plagioclase phenocrysts up to 1 mm long (Perry and Straub, 1996). Based on Sr and Nd isotopic compositions, elevated concentrations of rare earth elements, Sr, Ba, and Th, and lower Rb relative to typical alkali basalts, previous workers have concluded that Lathrop Wells magma was derived from an enriched lithospheric mantle source (Vaniman et al. 1982, Farmer et al. 1989, Perry et al., 1998).

Small but systematic geochemical differences occur between early and late erupted magmas as reflected in the two flow fields (Table 1; Perry and Straub 1996, Perry et al. 1998). Early lavas are generally 0-2% nepheline normative, while late lavas are generally 0-2% hypersthene normative, primarily because of slightly lower Na_2O content at the same SiO_2 content in the late lavas. Incompatible trace element differences between early and late flows show both relative depletion and enrichment in the later flows. Th and Rb values are 15-20% higher in the late flows, while Sr, Nd, and Sm values are 5-10% lower. Perry et al. (1998) tested several mechanisms to account for these differences including fractional crystallization, crustal contamination and magma mixing. They concluded that none of these mechanisms can account for the observed geochemical trends and hypothesized the differences are due to processes that occurred in the mantle source during melting and melt withdrawal. Nicholis and Rutherford (2004) studied phenocryst-melt equilibria of Lathrop Wells lava and nearby Crater Flat volcanic products, and concluded that magma-ascent rates exceeded 0.04 m/s to account for formation of microlitic plagioclase textures found in the lavas. They calculate that the ascending magma was near-water-saturated with temperature of ~975-1000°C and with ~1.2-4.6 wt% H_2O based upon their own analyses of melt inclusions and those of Luhr and Housh (2002).

The volcano consists of a scoria cone and two lava fields (Fig. 2; Valentine et al., 2005), and remnants of a scoria fallout deposit that extends up to ~20 km from the vent. The cone was 140 m high (before summit quarrying) with an elongate base and its summit encloses a crater that is partially filled by colluvium and eolian sediments. The outer cone slopes consist entirely of loose scoria lapilli, sparse blocks and bombs, and of eolian sediments that are mixed in the upper few decimeters. Several meters of scoria have been erosionally removed from the cone rim and moved down the cone slopes by creep and fluvial processes (Perry et al., 1998). Lava

flow fields extend from the base of the cone on its northeast, east, and south sides, covering an area of 1.95 km^2 with average flow thickness of ~15 m and steep flow fronts. The lavas were emplaced on the low-angle (1°-2°), south-sloping surface of the basin similar to lavas produced by the ~1 Ma volcanoes in nearby Crater Flat (Valentine et al., 2006), although at Lathrop Wells the lavas locally flowed around a low ridge of Miocene tuff that is partly straddled by the volcano.

The relative timing of emplacement of the cone, fallout deposits, and lava fields is shown schematically in Fig. 3. Early cone building was accomplished by Strombolian explosions from eruption along a short fissure that is now buried by the cone (Valentine et al., 2005; Valentine and Perry, 2006). This early explosive activity resulted in little, if any, fallout deposition beyond the cone itself, and was accompanied by effusion of lavas that formed the south lava field. Activity was soon confined to a single eruptive vent and became increasingly energetic, producing sustained eruption columns of well-fragmented, highly vesicular basalt lapilli and ash characteristic of violent Strombolian mechanisms. The bulk of the cone was built by this violent Strombolian activity (Valentine et al., 2005), along with emplacement of fallout deposits that buried most of the early, south lava field. The northeast lava field was emplaced late with respect to pyroclastic activity; these lavas overlie fallout deposits but also are locally (north of the cone) covered with a veneer of fallout. One of the last eruptive events recorded at the cone was a summit explosion, which deposited fist-size and smaller pieces of distinctive basalt-xenolith breccia around the cone base.

5. Products of the Strombolian eruptive phase

5.1. Early (lower) cone

Quarrying of the southern cone slope has exposed an early phase of the cone composed

of welded spatter and agglutinate (~40 m above the base level of the cone; Fig. 4). These deposits are dull red, massive to crudely bedded, partly welded bomb-and-coarse-lapilli agglutinate, and are the only deposits we have observed in the cone that have plagioclase phenocrysts. Clasts range from roughly equant, angular to subrounded lapilli and blocks (probably representing variably recycled fragments of broken bombs) to large (~1 m) fluidal spindle and ribbon bombs. Some small bombs have irregular, ragged shapes that fold around underlying clasts, indicating that the bombs were molten upon impact. Sparse bombs have cauliflower surface textures that indicate some quenching by wet steam or liquid water. In the quarry, deposits are partly welded but there is little compaction deformation of clasts. This facies is consistent with deposition of coarse bombs that traveled on relatively low ballistic paths with limited in-flight cooling, as well as ejecting recycled bombs and bomb fragments that avalanched into the vent, indicative of Strombolian eruptions (see McGetchin et al., 1974; Valentine et al., 2005). In quarry exposures this early cone-building facies is in sharp contact with, and mantled by, overlying beds of well-sorted scoria lapilli of the later violent Strombolian eruptions.

Although *in situ* exposures of the early cone-building facies are limited and transient because of quarry activities, features of the contemporaneous south lava field provide additional clues about the nature of the early cone. As described in Section 5.2, the many mounds of pyroclastic material dispersed across the lava field are the result of rafting of cone material atop lava flows. Most of the rafted mounds preserve facies (either intact or partly disintegrated during transport on the lavas) that are identical to the *in situ* facies described above. One large raft is an intact sequence of densely welded spatter grading upward over ~ 2 m into moderately welded bombs and lapilli. The densely welded spatter indicates that the early cone building included

periods of sustained, relatively rapid accumulation of hot, fluid clasts (Head and Wilson, 1989; Sumner et al., 2005). Some of the lavas produced during early cone building may have originated as clastogenic flows. These observations suggest that at cones with unexposed internal stratigraphy, rafted mounds on top of associated lava flows provide an indirect way to determine styles of pyroclastic activity within the cones (see also Holm, 1987). Additionally, the relative abundance of rafted mounds on the south lava field at Lathrop Wells indicates that slumping and cone "deconstruction" by rafting was a major part of the early cone building phase (see also Valentine et al., 2006).

5.2 South lava field

The south lava field extends ~800 m from the southern base of the cone (prior to quarry operations), implying an average effusion rate on the order of 1 m^3/s (Walker, 1973). The surface of the lava field is buried by fallout over much of proximal and medial portions. The lavas initially flowed directly southward around the west side of a small hill of Miocene ignimbrite, and then south-southeastward around the east side of the hill, to form a western and an eastern part of the lava field. The western part has margins characterized by lobes that are commonly 20-80 m wide and extend a few tens of meters to nearly 200 m from the main part of the lava field. Surface textures such as linear or arcuate squeeze-up ridges, lava tumuli, and ripply surface ridges (formed on the top of lava channels on the axes of long lobes) are more abundant toward the distal edges of the lava field where they are less obscured by the southward-thinning fallout deposits (Fig. 5). Flow fronts are clearly preserved and are characterized by steep margins, typically 2-4 m high, of blocky lava. Down stepping of marginal flow lobes as they extend outward onto the desert floor represents breakouts from the lobes. This indicates the presence of a tube network that fed lava toward distal margins and provided material for lateral

growth of the lava field (see also, for example, Pinkerton and Sparks, 1976; Valentine et al., 2006). One small lobe of lava (now buried by quarry tailings) extends ~100 m southwest of the cone base. This lobe and the western part of the south lava field are the only lavas that contain plagioclase phenocrysts and on this basis are inferred to be a very early lava of the same type that was erupted by Strombolian activity during early cone-building.

An additional characteristic of the south lava field is the presence of many mounds, typically 20-40 m in diameter and up to ~2 m high, of coarse pyroclastic material. There are four main types of mounds. One type is composed, on the crest of the mound, of partly welded, angular fragments with variable vesicularity. This mound type ranges from linear (~10 m long by 1-2 m wide) to circular in map view, and may represent lava-flow-top breccia that was uplifted as tumuli, although the detailed structure is indeterminate due to partial burial by the fallout scoria. The coarse breccia may have been pushed upward (driven by internal inflation of the underlying lava) so that it partly protrudes above the fallout deposits, or it may have been blanketed with fallout that has since been stripped off the steepest surfaces by erosion (e.g., Valentine et al., 2006). A second type of mound consists of loose, scattered accumulations of decimeter-sized ribbon and spindle bombs, and may also contain rotated slabs of agglutinate. A narrow dike-like lava squeeze-up, 20-30 cm thick and about 20 m long with an arcuate shape, occurs at the southern foot of one such mound (Fig. 6a). A third type of mound consists of a coherent mass of variably welded spatter and agglutinate that preserves original bedding (Fig. 6b,c). We interpret the latter two mound types to represent pyroclasts deposited in the main cone, during early Strombolian eruptions, that were subsequently dislodged by flowing lava and rafted to their final locations (see also Gutmann, 1979; Holm, 1987; Luhr and Simkin, 1993; Valentine et al., 2006). This is supported by the presence of plagioclase phenocrysts similar to

those found in the early cone deposits. The preservation and orientation of bedding in the final rafted mass depend upon the degree of welding of the original beds where they formed on the cone. Partial break-up of non- to partly welded masses during rafting could be expected. A final type of pyroclast mound is composed of jumbled blocks of very coarse spatter distributed in a circular pattern ~10-15 m in diameter, interpreted to be the collapsed remnants of a hornito (rootless spatter vent; note that this feature was mistakenly referred to as a "collapsed tumulus" by Valentine et al., 2005). The pyroclastic debris from each of these mounds, together with the fallout deposits that blanket most of the south lava field, combine to obscure the flow surfaces. Our interpretations of these different types of pyroclast mounds are consistent with observations of historical eruptions (e.g., Williams and Moore, 1976; Luhr and Simkin, 1993; Sumner, 1998) and interpretations of similar features at other small basaltic volcanoes (e.g., Gutmann, 1979; Holm, 1987; Valentine et al., 2006), but differ from previous workers at Lathrop Wells who inferred that the mounds were separate eruptive vents (Note that Perry et al., 1998 argued that the fact that some mounds have internally coherent magnetization is most consistent with an interpretation that they are vents, but we point out that many of the mounds obtained their magnetic signal when they cooled within the cone and retained this as they were carried intact atop the lavas.).

6. Products of the violent Strombolian phase

6.1 Cone deposits

The upper ~2/3 of the cone (see Fig. 4) is composed of beds typically ~10 cm to > 1 m thick that slope outward near the angle of repose (~30°) in lower exposures and shallow slightly with elevation. The beds range from planar over lateral distances of tens of meters, to lenticular. They are composed of relatively well-sorted, loose, vesicular scoria lapilli. Internal structure

within many planar beds, such as slight variation in grain sizes, can in many cases be traced continuously over tens of meters laterally and up slope, indicating deposition by fallout. Other planar beds have internal structure indicative of a component of grain avalanching, such as horizons rich in inversely-graded, clast-supported coarse lapilli, that are lenticular over a few meters distance. Near the top of the quarry some planar beds "roll over" to dip inward toward the crater center, while maintaining relatively constant thickness; others are truncated by ventward-dipping beds. The roll-over geometry is indicative of deposition by fallout mantling the cone. No welding is observed in this facies, including very proximal crater wall deposits exposed by quarrying, and fluidal bombs comprise a minor component of the deposits. Valentine et al. (2005) discussed the role of fallout from sustained violent Strombolian eruption columns in this phase of cone building (see also Riedel et al., 2003; Martin and Nemeth, 2006), as opposed to ballistic emplacement of coarse bombs during the earlier Strombolian phase that is consistent with the classical model of McGetchin et al. (1974).

Six meters below the south rim of the crater, quarrying temporarily exposed a 40-cm thick, well-sorted, laminated to thinly bedded, planar- and cross-stratified ash (median clast diameter $Md \approx 0.1$-0.2 mm; Fig. 7a,b), sandwiched between massive beds of poorly sorted, non-welded, clast-supported, angular scoria lapilli ($Md \approx 8$ mm; Fig. 7b). The lamellae, consisting of alternating coarse and fine ash, range from 3- to 15-mm thick and dip conformably 30° to 35° toward the crater. The unit pinches out within ~50 m to the west, and the eastern extent was covered. Upper and lower contacts are parallel to the internal bedding and no scouring is evident, although cross stratification indicates a component of lateral transport. Plastically deformed bedding that surrounds a 4-cm-diameter clast suggests the beds were moist during deposition. Scanning electron microscopic analysis reveals equant, rounded grains of tachylite

with smooth, glassy vesicle wall remnants and less abundant sideromelane. We infer that this ash was deposited by a localized density current mechanism, possibly partial collapse or heavy fallout from an ash-rich eruption column (for example, Taddeucci et al, 2004a,b, mentions observations of such processes during 2001 eruptions of Mt. Etna, Italy).

The cone and crater are elongate with an axis oriented N12°W. Before quarrying, the rim had two peaks on its opposing north and south sides, both higher than the west and east sides of the rim. Many cones around the world are asymmetric because of strong winds or directed fountaining during eruptions. In such cases one quadrant of the rim will be elevated. The two-peaked nature of the Lathrop Wells rim is difficult to explain by these mechanisms. Instead, we argue that the cone shape reflects the fact that rafting of cone material atop lava flows mainly occurred from the eastern base of the cone. The higher base level of the cone on its eastern side (see Section 8.1) reflects accumulation of lavas around one or more lateral breakouts (boccas, now buried by scoria) that were the source for the flows. Slumping of cone material onto departing lava flows removed material from the side of the cone, resulting in its elongate shape and reducing the height of the eastern rim. Accumulation of proximal fallout scoria during violent Strombolian eruptions healed or buried any scarps that may have been produced by slumping (see also Holm, 1987; Luhr and Simkin, 1993). If rafting had not occurred, we infer that the cone would have had a more circular base and rim, and that the southern and northern parts of the rim would have been connected along the eastern quadrant by a rim that maintained a constant, or gently northward-rising, elevation; the eastern flank would also have had a slope closer to the angle of repose instead of the 24° slope that it exhibits now. This interpretation builds upon earlier work (summarized in Perry et al., 1998) that inferred the elongate shape might partly reflect the orientation of a feeder dike/fissure (inherited from early cone building

eruptions). An additional process that might have contributed to the two-peaked characteristic of the rim is a change in wind direction during violent Strombolian eruptions (see Section 6.2).

6.2 Fallout deposits beyond the cone

Ten stratigraphic columns of fallout deposits beyond the cone were measured in pits (Fig. 8, Table 2). Erosion of the deposits in most areas, and burial beneath alluvial sediments in others, greatly limit detailed reconstruction of their distribution. Maximum measured fallout thickness is 304 cm in a section measured 700 m south of the vent, although deposits clearly thicken closer to the cone. Grain size data for the deposits (Fig. 9), along with characteristic planar-parallel bedding that mantles pre-existing topography (except for very steep lava surface features), are consistent with the interpretation that most of these deposits originated by fallout from sustained buoyant eruption columns. Individual beds range from centimeters to decimeters in thickness. Some are massive while others show reverse-to-normal grading indicative of waxing and waning eruption column events; indeed, each bed probably represents a pulse in explosive activity. Most beds have clast-supported textures. Some beds consist of angular or slightly ragged, glassy and highly vesicular clasts, many of which appear to be fragments of small ribbons; we interpret these beds to consist of juvenile clasts that might have been shredded from an annulus of magma in the conduit by the eruptive jet (as suggested for "pajarito" clasts at Parícutin; Pioli et al., submitted). Other beds are dominated by variably rounded and abraded scoria clasts that appear to have been recycled by avalanching and churning in the vent. The fallout deposits are virtually xenolith-free, with the exception of a layer that we refer to as "salt and pepper" (Columns F, E, and B, Fig. 8) that occurs near the base the sequence in the northern and northwestern quadrants of the fallout distribution (see isopachs on Fig. 2c). This distinctive layer contains a few percent of coarse ash-sized, Miocene tuff xenoliths.

Northwest of the cone the fallout deposits blanketed an arcuate hill of Miocene ignimbrite. Near the middle of the fallout sequence along the cone-facing flank of this hill (within distances of 200-300 m from the cone base) there is a sequence of laminated and cross-laminated ash (grain size parameters plotted on Fig. 9 for comparison with other units in the fallout sequence) that reaches 120 cm in thickness (Column D, Fig. 8). The deposit thins to the northeast and southwest and is only found in this limited area; its total volume amounts to less than 0.03% of the volume of eruptive products from the volcano. Cross laminations within the deposit indicate that its emplacement involved lateral transport with an active bed load. We consider that there are three possible origins for this deposit that is interbedded with otherwise normal fallout facies: (1) Short-lived hydrovolcanic activity that produced a pyroclastic surge (base surge) event during the violent Strombolian activity. Wind may have pushed the surge in the downwind direction (e.g., Self et al., 1980) and blocking of the density stratified current by the tuff hill may have focused deposition in that area (Valentine, 1987). Rounded quartz grains (comprising up to 5 vol% of the clasts) in the deposit might have been ejected by such eruptions from eolian deposits on the paleosurface beneath the volcano. However, the lack of any clear, correlative hydrovolcanic blast record in the well-exposed cone sequence and the lack of palagonitization of the deposits do not strongly support the hydrovolcanic mechanism. Correlation of this unit with the cross laminated deposit near the cone rim, see Section 6.1, cannot be ruled out, although we think it is unlikely that the two are related given their highly localized distribution in different directions from the crater. (2) Heavy fallout from an ash-rich eruption column (referred to as "local collapse" by Taddeucci et al., 2004b, in their observations of analogous processes at Mt. Etna) that was bent toward the N-NW by wind, may have produced a weak density current (see also Talbot et al., 1994, for a larger scale example). As in

the above mechanism this current may have been blocked by topography and thus preferentially deposited on the volcano-facing side of the hill. The presence of abraded ash particles (Fig. 10) and rounded quartz grains is consistent with a strong wind that could have bent the eruption column, added to the lateral component of flow in the weak density current, and also mixed in some eolian grains. (3) Strong wind blowing to the N-NW across recently-deposited fallout might have remobilized ash-sized particles and mixed with eolian particles, and deposited on the windward side of the hill much like the mechanism that has produced sand ramps around the bases of many hills and ridges in the area. This mechanism involves no eruptive mechanism at all (actually, it calls for a lull in pyroclastic activity which is consistent with different dispersal directions for individual fallout beds as discussed below) and provides a mechanism for both mixing eolian sand with basalt grains and substantially abrading the basalt grains. Given the limited preservation of the deposits it is difficult to distinguish between these mechanisms. The evidence does not support the inference by Wohletz (1986) that these laminated and cross laminated deposits record a major, initial hydrovolcanic phase of eruptions that produced a tuff ring.

Lateral correlation of individual layers is ambiguous for most of the fallout sequence at Lathrop Wells, but some variations and local correlations do provide clues about the dispersal of different parts of the sequence. For example there is a distinctive doublet of ash layers near the base of the sequence that probably correlates the lower beds of sections Y and those to south of the vent. This doublet is absent to the north and is replaced in sections F and E by the above-mentioned salt-and-pepper layer. This indicates that separate fallout units were dispersed in different directions, some to the south and some (most?) to the north. The isopach map (Fig. 2c) must be viewed as a composite result, and cannot be simply related to column height and wind

directions. Based upon analogy with historical eruptions that produced similarly-dispersed fallout beds (e.g., Hill et al., 1998; Arrighi et al., 2001), we infer that individual eruption column events might have reached sustained heights up to a few kilometers. Many stratigraphic columns have distinct zones in their mid-sections that are characterized by ash layers. Although in most places these are planar bedded and do not show any clear evidence of lateral transport (i.e., they were likely deposited by simple fallout), it is possible that they are lateral equivalents of the laminated and cross-laminated ash unit described in the previous paragraph. Fig. 8 presents the stratigraphic columns in a manner that "normalizes" them to a common datum that assumes this correlation of ash layers is true. However, we note that there are other potential interpretations and it would be difficult to prove such correlations.

6.3 Northeast lava field

The northeast lava flow field extends from the northeast base of the cone, reaching up to 400 m northward. This proximal portion of the lava field is mantled by fallout scoria from the violent Strombolian eruptive phase and has several pyroclast mounds on it, while the main eastern portion of the field has little scoria on its top but does overlie fallout deposits and has sparse pyroclast mounds. These relationships indicate that the lava field formed late relative to pyroclastic eruptions and might have continued growing after they had ceased. The pyroclast mounds rise 5-15 m above the surrounding lava surface and have rounded tops, and are characterized by loose scoria clasts in the large lapilli to small block size range and are blocky in shape. Only one mound that we observed contained larger clasts that are fragments of broken fluidal bombs, as well as large blocks of dense, poorly vesicular basalt up to 1 m in size. One mound in the proximal area has a lava squeeze-up on one of its margins.

Mounds of pyroclasts within the northeast lava field are apparently more aligned along flow direction of associated lava than those on the south lava field. Perry et al. (1998) considered the alignment of mounds, along with observations from trenching their margins, to indicate the trend of fissures and vents for surrounding lava flows. In contrast, we interpret the mounds to be material that was rafted from the cone by lava effusion during the violent Strombolian cone-building phase. This is consistent with the grain size and lack of agglutination in the mounds of the northeast lava field (compare with mounds on the south lava field that commonly are agglutinated or welded and retain some original bedding, having been scavenged from the early, Strombolian cone). The alignment of mounds simply reflects flow direction of proximal lavas that carried the rafts.

Northeast of the cone the medial to distal parts of the northeast lava field bend to the south to form an elongate platform about 1.6 km long (implying effusion rates up to ~4 m^3/s; Walker, 1973), the central part of which is ~25 m above the surrounding desert floor. The overall geometry of the lava field suggests that it was fed by lavas that vented from the northeastern base of the cone. As lavas accumulated near the foot of the cone, they were successively diverted to the east until they were able to "catch" the gentle southward slope of the paleotopography. Then the bulk of lava emplacement was toward the south, probably following a shallow fluvial paleochannel. As the platform thickened and lengthened it also widened as lobes of lava broke out from the flow margin. Such lobes are preserved along the northern and eastern margins of the northeast lava field (Fig. 11), where they are typically ~10 m wide, ~10-20 m long and have fronts ranging from 2-5 m high. Many of the lobes have axial grooves (~1-2 m wide) on their surfaces that may represent small collapsed lava tubes, and a few have ripply surface ridges. The common down-stepping, terrace-like nature of individual lobes (Fig. 12a)

suggests that many of the lobes extended outward by successive breakouts from their toes (toothpaste lava; Rowland and Walker, 1987; Rossi, 1997).

The lobe breakout mechanism described above suggests that lava tubes fed much of the lateral growth of the lava field and from this we infer that some portion of the thickness of the lava platform may result from inflation (see, for example, Luhr and Simkin, 1993), but stacking of flows on the growing platform was also an important factor in its thickening. Features such as those shown in Fig. 12b clearly demonstrate stacking of flow units. It is common for successively higher flow units to have margins that are inboard of the underlying unit's edge. This reflects the occurrence of slight topographic highs near the edges of flows formed by swelling of the flow margin and squeeze-ups as it came to a stop. Thus as an overriding flow approached the outer margin of the earlier flow it began to move uphill, halting before reaching the edge of the earlier unit. This process helped produce a platform that is thickest along the axis of the lava field and steps down in a terrace-like manner towards its outer edges. Some stacked flow units, however, drape over and extend beyond the margin of underlying units (e.g., Fig. 12c). These may form relatively narrow (20-40 m wide) channels where they flowed over the steep front of an underlying unit, and then fanned out to form a distributary set of lobes on the relatively flat desert floor. This is reminiscent, on a small scale, of observations at volcanoes such as Mt. Etna where lavas flowed through well-defined channels over steep slopes, and then feed broader lava fields at the break in slope (e.g., Duncan et al., 2004).

The surface of most of the northeast lava field, where its platform is thickest, is obscured by eolian sand sheets and dunes, but some original emplacement features can be distinguished. One of these is a 40-60 m wide, ~600 m long zone along the lava field axis that has a vaguely defined, coarse (~10-20 m wavelength) ripply surface texture (Fig. 11) caused by pressure ridges

on the crust of an axial lava channel. Away from this axial channel there are small pressure ridges and lava terraces. The latter are typically arcuate in shape, 1-2 m high and a few tens of meters long, and subparallel to the axial channel and lava field margins. Some of these terraces are likely the fronts of small overflows from the axial channel.

7. Volumes of eruptive products, xenolith content, and conduit size

Volumes of volcanic products were calculated by planimeter and using the thickness values mid-way between adjacent isopachs. The area covered by ≥ 1 cm of tephra is ~ 182 km^2. Volume of tephra fall enclosed by the 1 cm isopach is ~0.07 km^3. The total lava volume of 0.03 km^3 was obtained using a mean flow thickness of 15 m. The early (south) and later (northeast) flows were differentiated based on appearance, topographic expression, color aerial photography, and evaluation of recent aeromagnetic survey results (Perry et al., 2005); the south lava flow has volume of 0.013 km^3 and the N flow volume is 0.016 km^3. Approximation of the cone as having a circular base with a mean radius of 700 m yields a cone volume of ~0.02 km^3 (this approximately corrects for cone volume that was removed by rafting; see Section 6.1). Thus the ratio of fallout to cone volumes is ~3.5. As with most prehistoric basaltic eruptions, a large uncertainty for Lathrop Wells is associated with the tephra fallout volume (Pyle, 1995) caused by erosion or burial of much of its extent. The volumes reported here supersede those in Valentine et al. (2005) and Valentine and Perry (2006) and reflect a reassessment of the fallout volume.

Xenolith abundances were measured on eighteen 1-m^2 exposures of vertical quarry walls using the method of Valentine and Groves (1996). Xenolith types are dominated by light-colored, fine-grained Miocene tuffs, which reach ~335 m thickness beneath the site (Peterman and Spengler, 1994), and are be present as loose clasts and in cored bombs. The abundance is greatest in the lower (early) violent Strombolian deposits in the cone and decreases one to two

orders of magnitude in later scoria intervals (Fig. 13). The range of xenolith concentration values obtained at Lathrop Wells cone is consistent with that measured in deposits produced by magmatic fragmentation (predominantly Strombolian and Hawaiian mechanisms) at the Lucero volcanic field (New Mexico; Valentine and Groves, 1996), and is significantly lower than values reported for hydrovolcanic eruption facies in the Lucero and Hopi Buttes (Arizona) fields (Valentine and Groves, 1996; White, 1991). Doubik and Hill (1999, p. 60) used computer-assisted image analysis to derive an average abundance of 0.9 vol% for xenoliths > 1-mm diameter for the Lathrop Wells cone, about one order of magnitude larger than our average of 9.8×10^{-4}. However, the common occurrence of secondary carbonate and/or silica coatings on lapilli surfaces is a possible reason why their xenolith concentration estimate is higher than ours.

Combining the mean xenolith volume fraction from our data of 9.8×10^{-4} with the cone volume from the preceding paragraph, and assuming a cylindrical conduit through the 335 m thick Miocene tuff sequence, the average conduit diameter is ~16 m. If the fallout deposits and lavas are assumed to have a similar xenolith content (a conservative assumption because, as mentioned above, most fallout beds are virtually xenolith-free and xenoliths are quite sparse in the lavas) the added volume of xenoliths would imply a maximum average conduit diameter of about 21 m. In reality the conduit is probably widest near the Earth's surface and narrows with depth (e.g., Keating et al., submitted), but the lack of depth control of xenoliths within the 335 m Miocene interval does not allow us to estimate this shape.

No xenolith concentrations are observed within the cone or fallout sheet that indicate any significant conduit-clearing activity. Doubik and Hill (199, p. 60) noted that distinctive, small clasts of basaltic breccia with up to 50 vol% angular xenoliths of heterogeneous Miocene tuffs are scattered around the lower flanks of the cone (none of this type have been observed within

quarry walls). The clasts range up to 15-cm diameter but average is <5 cm. The occurrence is limited to the late (possibly last) deposits of the cone. The total volume (estimated < 5 m^3) of the breccia clasts is insignificant relative to the cone volume. Their occurrence likely indicates some local, late-time disruption along the feeder dike or conduit boundaries within the thick ignimbrite host rock beneath the cone, possibly related to effects of waning magma flux below the vent.

8. Post-eruptive features

8.1 Scoria cone

The extent of erosion of the scoria cone has been a subject of debate, with arguments for little erosional modification of the cone centering on the lack of an erosional apron surrounding the base of the cone (Wells et al., 1990), and upon the relatively low degree of rilling compared to parts of the fallout deposits beyond the cone that have been completely stripped from some surfaces (discussed in Section 8.2). Erosional features in the form of shallow rills (wavelengths of 10-20 m and depths of 1-2 dm) are present on the upper 40-60 m of the outer cone and inner crater slopes (Fig. 14). Well-developed garlands of coarser scoria clasts are abundant on the upper two-thirds of the cone slopes, an indication of creep processes. Trenching of the inner crater slopes and rim by Perry et al. (1998) revealed that the uppermost primary tephra unit within the crater is a ~1 m thick, black, primary scoria-fall deposit that overlies red oxidized scoria deposits with no evidence of any temporal break between the units. The black scoria unit does not extend to the crater rim but is truncated within the present inner crater wall by an erosional surface ~4 m vertically below the present rim. The contact between the black and the underlying red scoria deposit has a dip of 33°. Extrapolation of the basal contact of the black scoria would project ~7-8 m above the present rim surface, assuming that the contact maintained a constant 33° dip to the rim midpoint (Fig. 15). Analysis of digital elevation data from the cone

and extrapolation of slopes also indicates that up to 9 m of rim material may have been removed. Thus Perry et al. (1998) estimate that the rim of the crater (on its west side) has been lowered by 5-9 m by a combination of erosional rilling and creep.

The cone profile (Fig. 15a) departs from that of a symmetrical cone with slopes at the angle of repose (30-35°). Rounding of the rim is due to the erosional and creep processes described above. A subtle bulge on the western and northern slopes (between altitudes of 860-930 m on the west slope profiled in Fig. 15a) represents scoria mass that has crept from the rim as well as a component that has washed down the rill system. The east flank of the cone rises at an angle of only 24° to a rim that is nearly 20 m lower than the opposing (western) rim, reflecting cone slumping and rafting during eruptions (described above).

Wells et al. (1990) argued for a cone age of ~20 ka or less based upon the relatively low degree of rilling and absence of a cone apron, and comparison with relationships between cone morphology and age at other basaltic volcanoes in the Mojave Desert. We suggest that the onset of degradation processes in this arid setting is delayed for cones that were dominated by violent Strombolian eruptions in their late stages of growth. The resulting cone slopes are composed initially of loose scoria blocks and lapilli. For some time after eruptions have ceased, rain will simply infiltrate into this loose, porous material and will not nucleate as runoff. As eolian sediments accumulate in the upper few decimeters (see discussion in Section 8.3) the porosity and permeability of the surface, and thus the infiltration capacity, is reduced until runoff and resulting material transport can occur. Lathrop Wells cone is in the initial stages of this degradation. The eolian sediment also is a source of fines that can facilitate formation of small debris flows that play an important role in cone degradation (Wells et al., 1990). This lag time while eolian material accumulates contrasts with cones that have coarse, welded (relatively

impermeable) material on their slopes. In these cases runoff nucleates immediately after cone formation and degradation advances quickly. This dependence on initial surface textures may have complicated Wells et al.'s (1990) inferences about cone age. A topic of future research is to quantify this time lag and the implications for degradation-based age estimates (e.g., Wood, 1980b; Hooper and Sheridan, 1998).

8.2 Fallout deposits beyond the cone

The fallout deposits have evolved in three different ways according to the types of surfaces upon which they were deposited. Where fallout accumulated within ~200 m of the immediate foot of the scoria cone, and on top of the lava fields (particularly the south lava field), the top surface is both above the level of active fluvial deposition and the surface slopes are low. The former means that the fallout deposits have not been buried by sediments in these locations, and the latter implies that the fallout surface (top of the deposit) has experienced relatively little surface runoff (rilling) and/or creep processes. In such locations the dominant surficial process is that of accumulation of eolian sediment, infiltration of that sediment into pore spaces in the fallout deposits, and ongoing development of desert pavements (Valentine and Harrington, 2006). This process is described in more detail in Section 8.3.

The fallout has been buried in some places by fluvial sediments where it was deposited on the low, flat parts of the surrounding valley floors, but also locally eroded by fluvial channeling. This combination is most prevalent from ~300 m – 2 km immediately west and north of the Lathrop Wells cone. Depth of burial beneath coarse alluvial sediments (and finer playa-like deposits around the north edge of the northeast lava field; see below) typically amounts to ~20-50 cm.

Surficial processes have been more complex where fallout was deposited on slopes and ridges composed of Miocene tuff bedrock. In such settings much of the fallout has already been completely stripped, but in two more proximal locations the stripping process is still under way. One of these is the afore-mentioned hill immediately west and northwest of the cone. Here the fallout deposits have been eroded from the upper one-third of the slopes of the hill. The upper reaches of the remaining fallout are characterized by small, low-profile ridges of tephra that lap up onto bedrock and are partly littered with fragments of Miocene tuff that were transported from uphill locations by small debris flows. Currently runoff nucleates in the notches between the ridges and has formed gullies that extend tens of meters downslope in a process that is very similar to that described on La Fossa (Vulcano Island, Italy) by Ferrucci et al. (2005). As the slope shallows toward the base of the hill, the gullies transition into small, subdued alluvial fans. Typically the primary fallout deposits beneath these gullies are overlain by decimeter-thick, massive debris flow deposits (matrix-supported mixture of sand, scoria clasts, and angular fragments of Miocene tuff), which in turn are overlain by crudely laminated and cross-laminated deposits that exhibit cut-and-fill features, indicating transient, hyperconcentrated flows (similar to, but on a smaller scale than, deposits of localized hyperconcentrated flows documented by Valentine et al., 1998). Apparently the process of erosion of fallout deposits off slopes involves multiple stages of transport by debris and hyperconcentrated flows, formation of debris fans or small alluvial fans, and subsequent migration of runoff to the low points between these fans. As with remobilization of cone slope material (Section 8.1), the accumulation of eolian sand and silt within the upper decimeters of fallout deposits plays an important role in reducing porosity and permeability to facilitate runoff, and in providing fines that facilitate transport via debris flows.

8.3 Lava fields

Post-eruptive surficial features have evolved differently on the two lava fields due to their different original surfaces, and provide an important snapshot at an earlier stage relative to similar, ~1 Ma lava surfaces in Crater Flat (Valentine et al., 2006). Because of a mantle of fallout deposits in addition to abundant rafted pyroclastic material on the south lava field, it has a more subdued surface than that of the northeast lava field. This difference in the original volcanic surfaces has also played an important role in the post-eruptive geomorphic evolution of the lavas. Understanding the effects of initial conditions or textures on geomorphic processes is critical in attempting to determine relative ages of surfaces. For example, Bradshaw and Smith (1994) assumed that differences in surface morphology of lava fields at the ~1 Ma volcanoes in Crater Flat were evidence of significant age differences of eruptive units within individual small-volume volcanoes. Wells et al. (1990) came to a similar conclusion about the two lava fields at Lathrop Wells, stating: "Those flows along the southwestern edge of the cone appear to be the oldest, whereas flows along the northeastern part of the cone appear to be the youngest." They concluded that the lava fields were produced by polycyclic eruptions separated by significant periods of time (although not explicitly stated, the implication was 1,000s to 10,000s of years) based upon the different lava field morphologies. In reality, the individual volcanoes both in Crater Flat and at Lathrop Wells are monogenetic (erupted over time frames of months to years) and the geomorphic differences were controlled by variations in initial conditions.

In more humid climates, soils form on volcanic deposits mainly by a combination of in situ weathering of the parent material and accumulation of organic material. In contrast, soil formation in the arid to semi-arid Mojave Desert is dominated by deposition of eolian sediment in the fine sand to silt size range (e.g., McFadden et al., 1987, 1998). The style of eolian sedimentation is in turn intimately linked with the development of desert pavement (a mosaic of

lapilli-sized clasts on the surface of a desert soil). Valentine and Harrington (2006) described the development of soils and desert pavements on fallout lapilli deposits as a three stage process: (1) primary deposition of fallout lapilli beds; (2) deposition of eolian sediment on and around surface clasts and infiltration of the sediment into interclast pore spaces in the uppermost decimeters of the pyroclastic deposit (by a combination of mechanical movements associated with wetting, drying, freezing, and thawing, and by bioturbation); (3) aggradation of clean eolian sediment above the fallout deposit after pore space is completely clogged, and lifting of the surface layer of clasts as a desert pavement. Subsequent geochemical processes cause additional zonation within the eolian soil (see McFadden et al., 1998, for review). Based upon field observations at Lathrop Wells volcano and at the nearby, ~1 Ma Red Cone volcano, Valentine and Harrington (2006) determined that this process must occur over many tens of thousands of years if the parent material is well-sorted scoria lapilli.

A key element of the above sequence of processes is that the desert pavement serves to trap eolian sediments and stabilize them with respect to later remobilization by wind. On a surface initially covered with abundant lapilli, clasts are immediately available for formation of desert pavement. This is the case with the south lava flow field. Most of its surface is covered by a maturing desert pavement that is underlain by a 20-40 cm-thick zone of mixed scoria and eolian sediment (the second stage discussed in the previous paragraph; Valentine and Harrington, 2006). If, on the other hand, such clasts are rare or absent (e.g., bare rock), pavement and resulting stabilization will be unable to develop until mechanical weathering of the surface has produced clasts from which a pavement can form; eolian sediment will be easily remobilized. This is the case with the northeast lava field, which is largely covered by an active dune field. Lava crags and other surface irregularities act as nuclei for dunes; abundant eolian sediment is

trapped on the surface of the lava field but only temporarily, unlike that which is permanently trapped beneath desert pavements of the south lava field. Early-stage formation of pavement material is actively taking place by mechanical weathering of lava highs (e.g., Fig. 16). Eventually this weathering process, combined with eolian accumulation in low spots, will result in a smooth, variably paved surface for the lava field (as described at the Cima volcanic field by Wells et al., 1985, and at the ~1 Ma basaltic volcanoes of Crater Flat by Valentine et al., 2006). Note that the small portions of the northeast lava field that have pyroclastic material (either directly deposited by fallout or rafted into place) have subdued topography and pavement similar to that of the south lava field (Valentine and Harrington, 2006).

The northeast lava field filled and raised the topography of the small fault-block-bounded valley occupied by the volcano and blocked a drainage from the north. We infer that several meters of alluvial sediment accumulated just to the north of the lava field, which partly buried some low-lying flow lobes (see Fig. 12c). It is likely that a lake (possibly ephemeral) formed in this area, as indicated by a small playa. As lake level rose, it overtopped the low point of the natural dam that was formed by the lavas and adjacent ridge (fault block) of Miocene ignimbrite, cutting a new channel through the ridge and around the eastern margin of the lava field.

9. Summary and conclusions

The Lathrop Wells volcano, despite its relatively small volume, displays a wide range of eruptive processes (Fig. 17). These range from relatively weak Strombolian explosions of coarse, ballistic bombs to sustained eruption columns of well-fragmented, vesicular scoria lapilli. Pyroclastic facies range from coarse, variably welded agglutinate rich in fluidal clasts to well sorted fallout beds and localized surge or surge-like units. Lava effusion occurred during both Strombolian and violent Strombolian explosive activity (Valentine et al., 2005). As with the

nearby ~1 Ma volcanoes in Crater Flat (Valentine et al., 2006), early lavas flowed southward down a gently sloping valley floor (although at Lathrop Wells this was slightly complicated by the presence of a low ridge of Miocene tuff that extended southward from the main vent area). The early lavas built a platform through a combination of inflation and flow-unit stacking; eventually this reversed the topography around the base of the cone such that later lavas were diverted northward and eastward until they encountered an unobstructed slope or a drainage channel down which they subsequently flowed. Early lavas were more likely to raft segments of the cone from its weaker down-slope (south) side, while later lavas rafted less material because of the buttressing effect of the sloping ground beneath the cone (Valentine et al., 2006). Previous authors (summarized in Perry et al., 1998) inferred that the scoria mounds scattered across the lava fields are separate vents, which in turn implies multiple feeder dikes and conduits beneath the volcano's footprint. We interpret these mounds as rafted cone material and conclude that there was only one feeder dike/fissure and one main conduit from which all eruptive products emanated, with shallow (near the interface between cone and substrate), lateral breakouts from that conduit that fed lava flow fields.

Comparison of the Lathrop Wells cone height with the growth rates of historically observed scoria cones (Fig. 7 of Wood, 1980a) suggests that the cone could have been constructed over a period of 1-100 days of explosive activity, most likely a time scale of a few weeks, and the fallout deposits beyond the cone were deposited during the later (violent Strombolian) cone building activity. The south lava field would have required ~150 days to accumulate based upon a continuous effusion rate of about 1 m^3/s, while the northeast lava field would require ~45 days at a continuous effusion rate of 4 m^3/s (note that the effusion might have been pulsatory, as suggested by Valentine et al., 2006, which would extend the durations). These

time scales, although very rough, indicate that the volcano might have been active for as little as ~7 months, and that explosive cone-building activity occurred during only part of that time. Because much of the northeast lava field has little or no fallout scoria on its top it seems likely that much of its emplacement continued after pyroclastic activity had ceased.

The complexity of the Lathrop Wells eruption, given that the major element composition changed very little throughout, indicates that fluid dynamic processes such as vesiculation and bubble coalescence, gas loss to country rocks, and varying degrees of separation in the two-phase eruptive mixture (e.g., Pioli et al., in review) to produce simultaneous violent Strombolian columns and lava effusion, are of fundamental importance in determining eruption processes at scoria cone volcanoes. This points to a need for detailed theoretical and field studies of the subsurface plumbing, crystallization and vesiculation textures, and heat and mass transfer between rising magma and country rocks, in order to quantify the conditions that lead to one eruption process versus another given little change in the composition of the silicate melt.

The different volcanic surfaces left by the eruption that formed the Lathrop Wells volcano have been modified by a variety of geomorphic processes. As mentioned earlier, Lathrop Wells provides an earlier-time snapshot of these processes relative to those observed at the older volcanoes in Crater Flat (Valentine et al., 2006). The fact that such volcanoes initially produce a variety of surfaces, along with the fact that the eruptions can be accurately dated by techniques such as $^{40}Ar/^{39}Ar$, suggests that the combination of quantitative physical volcanological and geomorphic characterization of successively older volcanoes can provide much insight into the rates of surficial processes as a function of initial condition in a given environmental setting (building, for example, on the work of Wells et al., 1985; McFadden et al., 1987, 1998; Valentine and Harrington, 2006).

If a future volcanic event occurs at Yucca Mountain and intersects the proposed repository (250-350 m depth), based upon the phenomena that created the Lathrop Wells volcano we anticipate the following features: (1) The total volume of eruptive products will be ~0.1 km^3 and will be partitioned such that about 1/3 of the volume is erupted as lavas and the rest is erupted as pyroclasts, most of which would be dispersed by eruption columns up to a few km high. (2) The event will be from one main feeder dike and conduit, up to ~20-25 m in diameter at repository depth, with shallow lateral breakouts (as opposed to multiple feeder dikes and conduits) that feed lava flows. (3) Based upon the violent Strombolian nature of much of the eruption, we anticipate that explosivity of the initial interaction with repository tunnels (or drifts) and subsequent eruptive dispersal could be high if the trachybasaltic magmas have significant volatiles (see Woods et al., 2002; Dartevelle and Valentine, 2005). Hydrovolcanic explosions might occur if shallow groundwater is available, but this would be relatively minor based upon the small fraction of products at Lathrop Wells that might be of hydrovolcanic origin and the near absence of evidence for such activity in other volcanoes of Crater Flat (Valentine et al., 2006). (4) Fallout tephra, potentially contaminated by entrained radioactive waste, would be stripped from slopes (particularly bedrock slopes) and transported away by fluvial processes, with only thick proximal deposits remaining after tens of thousands of years, while fallout deposited on relatively flat surfaces may be buried and immobilized by an accumulation of eolian or fluvial sediments or locally incised by channels and transported downstream. Cone deposits might be relatively stable for several tens of thousands of years before degradation processes set in.

Acknowledgements

This work was supported by the U.S. Department of Energy's Yucca Mountain Project, which is

managed by Bechtel-SAIC, LLC. We thank Mike Cline for his management support of volcanic risk studies at Yucca Mountain.

References

Arrighi, S., Principe, C., Rosi, M., 2001. Violent strombolian and subplinian eruptions at Vesuvius during post-1631 activity. Bull. Volcanol. 63, 126-150.

Bradshaw, T.K., Smith, E.I., 1994. Polygenetic Quaternary volcanism at Crater Flat, Nevada. J. Volcanol. Geotherm. Res. 63, 165-182.

Champion, D.E., 1991. Volcanic episodes near Yucca Mountain as determined by paleomagnetic studies at Lathrop Wells, Crater Flat, and Sleeping Butte, Nevada. In: Proceedings High Level Radioactive Waste Management Conference, Las Vegas, Nevada (American Nuclear Society, La Grange Park, Illinois), 61-67.

Crowe, B.M., 1986. Volcanic hazard assessment for disposal of high-level radioactive waste, In: Active Tectonics (National Academy Press, Washington, D.C.), 247-260.

Crowe, B.M., Carr, W.J., 1980. Preliminary assessment of the risk of volcanism at a proposed nuclear waste repository in the southern Great Basin. U.S. Geological Survey Open-File Report 80-375, 15 pp.

Crowe, B.M., Perry, F.V., 1989. Volcanic probability calculations for the Yucca Mountain site: estimation of volcanic rates. In: Proceedings Nuclear Waste Isolation in the Unsaturated Zone, Focus '89, Symposium, American Nuclear Society, 326-334.

Crowe, B., Self, S., Vaniman, D., Amons, R., Perry, F., 1983. Aspects of potential magmatic disruption of a high-level radioactive waste repository in southern Nevada. J. Geol. 91, 259-276.

Crowe, B.M., Wohletz, K.H., Vaniman, D.T., Gladney, E., Bower, N., 1986. Status of volcanic hazard studies for the Nevada Nuclear Waste Storage Investigations. Los Alamos Nat. Lab. Rep. LA-9325-MS, vol. II, 101 pp.

Crowe, B., Perry, F., Geissman, J., McFadden, L., Wells, S., Murrell, M., Poths, J., Valentine, G.A., Bowker, L., Finnegan, K., 1995. Status of volcanism studies for the Yucca Mountain Site Characterization Project. Los Alamos Nat. Lab. Rep. LA-12908-MS, 363 pp.

Crowe, B.M., Valentine, G.A., Perry, F.V., Black, P.K., 2006. Volcanism: the continuing saga. In: McFarlane, A.M., Ewing, R.C. (Editors), Uncertainty Underground: Yucca Mountain and the Nation's High-Level Nuclear Waste, MIT Press, Cambridge, Massachusetts, 131-148.

Dartevelle, S., Valentine, G.A., 2005. Early-time multiphase interactions between basaltic magma and underground openings at the proposed Yucca Mountain radioactive waste repository. Geophys. Res. Let. 32, L22311, doi:10.1029/2005GL024172.

Doubik, P., Hill, B.E., 1999. Magmatic and hydromagmatic conduit development during the 1975 Tolbachik Eruption, Kamchatka, with implications for hazards assessment at Yucca Mountain, NV. J. Volcanol. Geotherm. Res 91, 43-64.

Duncan, A.M., Guest, J.E., Stofan, E.R., Anderson, S.W., Pinkerton, H., Calvari, S., 2004. Development of tumuli in the medial portion of the 1983 aa flow-field, Mount Etna, Sicily. J. Volcanol. Geotherm. Res 132, 173-187.

Farmer, G.L., Perry, F.V., Semken, S., Crowe, B., Curtis, D., DePaolo, D.J., 1989. Isotopic evidence on the structure and origin of subcontinental lithospheric mantle in southern Nevada. J. Geophys. Res. 94, 7885-7898.

Ferrucci, M., Pertusati, S., Sulpizio, R., Zanchetta, G., Pareschi, M.T., Santacroce, R., 2005. Volcaniclastic debris flows at La Fossa Volcano (Vulcano Island, southern Italy): Insights for

erosion behavior of loose pyroclastic material on steep slopes. J. Volcanol. Geotherm. Res., v. 145: 173-191.

Fleck, R.J., Turrin, B.D., Sawyer, D.A., Warren, R.G., Champion, D.E., Hudson, M.R., Minor, S.A., 1996. Age and character of basaltic rocks of the Yucca Mountain region, southern Nevada. J. Geophys. Res. 101, 8205-8227.

Gutmann, J.T., 1979. Structure and eruptive cycle of cinder cones in the Pinacate volcanic field and the controls of Strombolian activity. J. Geology 87, 448-454.

Head, J.W., Wilson, L., 1989. Basaltic pyroclastic eruptions: influence of gas-release patterns and volume fluxes on fountain structure, and the formation of cinder cones, spatter cones, rootless flows, lava ponds, and lava flows. J. Volcanol. Geotherm. Res. 37, 261-271.

Heizler, M.T., Perry, F.V., Crowe, B.M., Peters, L., Appelt, R., 1999. The age of the Lathrop Wells volcanic center: An $^{40}Ar/^{39}Ar$ dating investigation. J. Geophys. Res. 104, 767–804, doi: 10.1029/1998JB900002.

Hill, B.E., Connor, C.B., Jarzemba, M.S., La Femina, P.C., Navarro, M., Strauch, W., 1998. 1995 eruptions of Cerro Negro volcano, Nicaragua, and risk assessment for future eruptions: Geol. Soc. Am. Bull. 110, 1231-1241.

Holm, R.F., 1987. Significance of agglutinate mounds on lava flows associated with monogenetic cones: An example at Sunset Crater, northern Arizona. Geol. Soc. Am. Bull. 99, 319-324.

Hooper, D.M., Sheridan, M.F., 1998. Computer simulation models of scoria cone degradation. J. Volcanol. Geotherm. Res. 83, 241-267.

Jarzemba, M.S., 1997. Stochastic radionuclide distributions after a basaltic eruption for performance assessments of Yucca Mountain. Nuc. Technol. 118, 132-141.

Keating, G.N., Pelletier, J., Valentine, G.A., submitted. How good is good enough: evaluating sufficiency in a tephra dispersal model as part of a risk assessment framework. Geophys. Res. Lett.

Keating, G.N., Valentine, G.A., Krier, D., Perry, F.V., submitted. Shallow plumbing systems for small-volume basaltic volcanoes. J. Volcanol. Geotherm. Res.

Luhr, J.F., Housh, T.B., 2002. Melt volatile contents in basalts from Lathrop Wells and Red Cone, Yucca Mountain Region (SW Nevada): Insights from glass inclusions. Eos Trans. Am. Geophys. Union 83, Abs. V22A-1221.

Luhr, J.F., Simkin, T (Editors), 1993: Parícutin, the volcano born in a Mexican cornfield. Phoenix, Geoscience Press, Inc., 427 pp.

Martin, U., Nemeth, K., 2006. How Strombolian is a "Strombolian" scoria cone? Some irregularities in scoria cone architecture from the Transmexican Volcanic Belt, near Volcán Ceboruco, (Mexico) and Al Haruj (Libya). J. Volcanol. Geotherm. Res. 155, 104-118.

McFadden, L.D., Wells, S.G., Jercinovich, M.J., 1987. Influences of eolian and pedogenic processes on the origin and evolution of desert pavements. Geology 15, 504-508.

McFadden, L.D., McDonald, E.V., Wells, S.G., Anderson, K., Quade, J., Forman, S.L., 1998. The vesicular layer and carbonate collars of desert soils and pavements: formation, age, and relation to climate change. Geomorphology 24, 101-145.

McGetchin, T.R., Settle, M., Chouet, B.A., 1974. Cinder cone growth modeled after Northeast Crater, Mount Etna, Sicily. J. Geophys. Res. 79, 3257-3272.

Nicholis, M.G., Rutherford, M.J., 2004. Experimental constraints on magma ascent rate for the Crater Flat volcanic zone hawaiite. Geology 32, 489-492.

Pelletier, J.D., M.L. Cline, S.B. DeLong, C.D. Harrington, Keating, G.N., submitted. Dispersion of channel-sediment contaminants in bedload-dominated distributary fluvial systems: Application to fluvial tephra redistribution following a potential volcanic eruption at Yucca Mountain. Geol. Soc. Am. Bull.

Perry, F.V., Straub, K.T., 1996. Geochemistry of the Lathrop Wells volcanic center. Los Alamos Nat. Lab. Rep. LA-13113-MS.

Perry FV, Crowe BM, Valentine GA, Bowker LM (Editors), 1998, Volcanism studies: final report for the Yucca Mountain Project. Los Alamos Nat. Lab. Rep. LA-13478-MS, 554 pp.

Perry, F.V., Cogbill, A.H., Kelley, R.E., 2005. Uncovering buried volcanoes at Yucca Mountain: New data for volcanic hazard assessment. Eos Trans. Am. Geophys. Union 86, 485, 488.

Peterman, Z.E., Spengler, R.W., 1994. Geochemistry of outcrop samples from the Raven Canyon and Paintbrush Canyon reference sections, Yucca Mountain, Nevada. U.S. Geol. Survey Open File Report 94-550, 27 pp.

Pinkerton, H., Sparks, R.S.J., 1976. The 1975 sub-terminal lavas, Mount Etna: a case history of the formation of a compound lava field. J. Volcanol. Geotherm. Res. 1, 167-182.

Pioli, L., Cashman, K., Wallace, P., Johnson, E., Delgado-Grenados, H., Rosi, M., in press. Parícutin revisited: A new look at violent Strombolian eruptions. Geology.

Potter, C.J., Sweetkind, R.P., Drake II, R.M., Taylor, E.M., Fridrich, C.J., San Juan, C.A., Day, W.C., 2002. Geologic map of the Yucca Mountain region, Nye County, Nevada. U.S. Geol. Survey Investigations Series I-2755.

Pyle, D. M., 1995. Assessment of the minimum volume of tephra fall deposits. J. Volcanol. Geotherm. Res. 69, 379-382.

Riedel, C., Ernst G.G.J., Riley, M., 2003. Controls on the growth and geometry of pyroclastic constructs. J. Volcanol. Geotherm. Res. 127, 121-152.

Rossi, M.J., 1997. Morphology of the 1984 open-channel lava flow at Krafla volcano, northern Iceland. Geomorphology 20, 95-112.

Rowland, S.K., Walker, G.P.L., 1987. Toothpaste lava: characteristics and origin of lava structural type transitional between pahoehoe and aa. Bull. Volcanol. 49, 631-641.

Sawyer, D.A., R.J. Fleck, M.A. Lanphere, R.G. Warren, D.E. Broxton, M.R. Hudson, 1994. Episodic caldera volcanism in the Miocene southwestern Nevada volcanic field: revised stratigraphic framework, $^{40}Ar/^{39}Ar$ geochronology, and implications for magmatism and extension. Geol. Soc. Am. Bull. 106, 1304-1318.

Self, S., Kienle, J., Huot, J.-P., 1980. Ukinrek maars, Alaska, II. Deposits and formation of the 1977 craters. J. Volcanol. Geotherm. Res. 7, 39-65.

Sumner, J.M., 1998. Formation of clastogenic lava flows during fissure eruption and scoria cone collapse: the 1986 eruption of Izu-Oshima Volcano, eastern Japan. Bull. Volcanol. 60, 195-212.

Sumner, J.M., Blake, S., Matela, R.J., Wolff, J.A., 2005. Spatter. J. Volcanol. Geotherm. Res.142, 49-65.

Taddeucci, J., Pompilio, M., Scarlato, P., 2004a. Conduit processes during the July-August 2001 explosive activity at Mt. Etna (Italy): Inferences from glass chemistry and crystal size distribution of ash particles. J. Volcanol. Geotherm. Res. 137, 33-54, doi:10.1016/j.jvolgeores.2004.05.011.

Taddeucci, J., Spieler, O., Kennedy, B., Pompilio, M., Dingwell D., Scarlato, P., 2004b, Experimental and analytical modeling of basaltic ash explosions at Mounta Etna, Italy, 2001. Jour. Geophys. Res. 109, 1-9.

Talbot, J.P., Self, S., Wilson, C.J.N., 1994. Dilute gravity current and rain-flushed ash deposits in the 1.8-ka Hatepe Plinian deposit, Taupo, New Zealand. Bull. Volc. 56, 538-551.

Turin, B.D., Champion, D.E., Fleck, R.J., 1991. $^{40}Ar/^{39}Ar$ age of the Lathrop Wells volcanic center, Yucca Mountain, Nevada. Science 253, 654-657.

Turin, B.D., Champion, D.E., Fleck, R.J., 1992. Measuring the age of the Lathrop Wells volcanic center at Yucca Mountain: Response to comment on $^{40}Ar/^{39}Ar$ age of the Lathrop Wells volcanic center, Yucca Mountain, Nevada. Science 257, 556-558.

Valentine, G.A., 1987. Stratified flow in pyroclastic surges. Bull. Volcanol. 49, 616-630.

Valentine, G.A., Groves, K.R., 1996. Entrainment of country rock during basaltic eruptions of the Lucero volcanic field, New Mexico. J. Geol. 104, 71-90.

Valentine, G.A., Harrington, C.D., 2006. Clast size controls and longevity of Pleistocene desert pavements at Lathrop Wells and Red Cone volcanoes, southern Nevada. Geology 34, 533-536.

Valentine, G.A., Krogh, K.E.C., 2006. Emplacement of shallow dikes and sills beneath a small basaltic volcanic center - the role of pre-existing structure (Paiute Ridge, southern Nevada, USA). Earth Planet. Sci. Lett. 246, 217-230.

Valentine, G.A., Perry, F.V., 2006. Decreasing magmatic footprints of individual volcanoes in a waning basaltic field. Geophys. Res. Lett., doi:10.1029/2006GL026743.

Valentine, G.A., Palladino, D.M., Agosta, E., Taddeucci, J., Trigila, R., 1998. Volcaniclastic aggradation in a semi-arid environment, northwestern Vulcano Island, Italy. Geol. Soc. Am. Bull. 110, 630-643.

Valentine, G.A., Krier, D., Perry, F.V., Heiken, G., 2005. Scoria cone construction mechanisms, Lathrop Wells volcano, southern Nevada, USA. Geology 33, 629-632.

Valentine, G.A., Perry, F.V., Krier, D., Keating, G.N., Kelley, R.E., Cogbill, A.H., 2006. Small-volume basaltic volcanoes: eruptive products and processes, and post-eruptive geomorphic evolution in Crater Flat (Pleistocene), southern Nevada. Geol. Soc. Am. Bull, doi:10.1130/B25956.

Vaniman, D., and Crowe, B., 1981. Geology and petrology of the basalts of Crater Flat: applications to volcanic risk assessment for the Nevada Nuclear Waste Storage Investigations. Los Alamos Nat. Lab. Rep. LA-8845-MS, 67 pp.

Vaniman, D.T., Crowe, B.M., Gladney, E.S., 1982. Petrology and geochemistry of hawaiite lavas from Crater Flat, Nevada. Contrib. Mineral. Petrol. 80, 341–357, doi: 10.1007/BF00378007.

Walker, G.P.L., 1973. Lengths of lava flows. Phil. Trans. Roy. Soc. Lond. Series A 274, 107-118.

Wells, S.G., Dohrenwend, J.C., McFadden, L.D., Turin, B.D., Mahrer, K.D., 1985. Late Cenozoic landscape evolution on lava flow surfaces of the Cima volcanic field, Mojave Desert, California. Geol. Soc. Am. Bull. 96, 1518-1529.

Wells, S.G., McFadden L.D., Renault, C.E., Crowe, B.M., 1990. Geomorphic assessment of late Quaternary volcanism in the Yucca Mountain area, southern Nevada: Implications for the proposed high-level radioactive waste repository. Geology 18, 549-553.

Wells, S.G., McFadden, L.D., Renault, C.E., Crowe, B.M., 1991. Reply on Geomorphic assessment of late Quaternary volcanism in the Yucca Mountain area, southern Nevada: Implications for the proposed high-level radioactive waste repository – Reply. Geology 19, 661-662.

Wells, S.G., Crowe, B.M., McFadden, L.D., 1992. Measuring the age of the Lathrop Wells volcanic center at Yucca Mountain: Comment on $^{40}Ar/^{39}Ar$ age of the Lathrop Wells volcanic center, Yucca Mountain, Nevada. Science 257, 555-556.

White, J.D.L., 1991. Maar-diatreme phreatomagmatism at Hopi Buttes, Navajo Nation (Arizona), USA. Bull. Volcanol. 53, 239-258.

Williams, R.S., Moore, J.G., 1976. Man against volcano: The eruption on Heimaey, Vestmannaeyjar, Iceland. U.S. Geol. Survey Pub., 33 pp.

Wohletz, K.H., 1986. Explosive magma-water interactions: thermodynamics, explosion mechanisms, and field studies. Bull. Volcanol. 48, 245-264.

Wood, C.A., 1980a. Morphometric evolution of cinder cones. J. Volcanol. Geotherm. Res. 7, 387-413.

Wood, C.A., 1980b. Morphometric analysis of cinder cone degradation. J. Volcanol. Geotherm. Res. 8, 137-160.

Woods, A.W., Sparks, S., Bokhove, O., LeJune, A.-M., Connor, C.B., Hill, B.E., 2002. Modeling magma-drift interaction at the proposed high-level radioactive waste repository at Yucca Mountain, Nevada, USA. Geophys. Res. Lett. 29, doi:10.1029/2002/GL014665

Zreda, M.G., Phillips, F.M., Kubik, P.W., Sharma, P., Elmore, D., 1993. Cosmogenic ^{36}Cl dating of a young basaltic eruption complex, Lathrop Wells, Nevada. Geology 21, 57-60.

Figure Captions

Fig. 1. Digital elevation model of the Yucca Mountain area showing distribution of Plio-Pleistocene basaltic volcanoes, caldera outlines from mid-Miocene activity (Wahl et al., 1997), and major basins (Crater Flat, Jackass Flat). Pliocene volcanoes are Thirsty Mountain (TM), Buckboard Mesa (BM), and Pliocene Crater Flat (PCF). Pleistocene volcanoes in Crater Flat (LC – Little Cones, RC – Red Cone, BC – Black Cone, MC – Makani Cone) are ~1 Ma (Fleck et al., 1996; Perry et al., 1998; Valentine et al., 2006). Little Black Peak (LBP) and Hidden Cone (HC) are ~0.32 and 0.37 Ma, respectively (Fleck et al., 1996). Lathrop Wells volcano (LW) is ~80 ka (Heizler et al., 1999). Figure modified from Valentine and Perry (2006).

Fig. 2. Distribution of volcanic products at Lathrop Wells. (a) Aerial photo of the Lathrop Wells volcano. (b) Geologic map of the volcano (modified from Perry et al., 1998). (c) Inferred fallout distribution overlain on a digital elevation model. Contours represent fallout isopachs (approximate, given incomplete preservation and exposure of the deposits), units in cm. Inset shows possible regional extent based upon thin (~1 cm) remnants of ash in distal locations. Lettered stations refer to stratigraphic columns in Fig. 8.

Fig. 3. Schematic diagram showing the relative timing of emplacement of scoria cone, fallout, and lava fields at the Lathrop Wells volcano.

Fig. 4. Photograph of cone-building deposits associated with the early, Strombolian phase of activity, overlain by cone deposits from the later violent Strombolian phase (as exposed by quarry operations in late 2001).

Fig. 5. Map of western part of the south lava field, showing lobate flow margins (solid lines) and pressure ridge and squeeze-up features (dashed lines).

Fig. 6. Examples of two types of pyroclast mounds on the south lava field. (a) Mound consisting of broken slabs or masses of partly welded agglutinate. This example has a narrow, arcuate squeeze-up (rootless dike) along its leading edge (emplacement direction was toward the photographer). (b) Pyroclast mound composed of an intact, tilted block of bedded spatter and agglutinate, near eastern margin of south lava field. Black lower portion is densely welded spatter. Red upper part is moderately welded agglutinate. The block tilts downward away from the photographer. (c) Internal structure of an intact pyroclast mound, showing steeply tilted bedding of partly welded agglutinate. A thin layer of spatter crosses the middle of the meter stick. A thick mantle of fallout lapilli beds (from violent Strombolian eruptions at the cone) covered this rafted block prior to quarrying activities, such that it had a subdued, rounded morphology.

Fig. 7. (a) Photograph of cross-stratified ash deposit interbedded with scoria lapilli deposits in upper cone. (b) Cumulative grain size distribution for cross-stratified ash deposit (samples DK-LW-74,76) and overlying scoria lapilli bed (sample DK-LW-76) that is typical of the upper cone-forming deposits.

Fig. 8. Stratigraphic columns (locations shown in Fig. 2c and Table 2) of fallout deposits at ten sites ranging up to 2 km from the vent. Columns are drawn with respect to an inferred common datum (stratigraphic level) that corresponds to the emplacement of the localized cross-laminated ash unit described in Section 6.2, assuming that thin, planar ash layers observed elsewhere correlate with that unit. The authors note that this is not considered to be a unique interpretation.

Fig. 9. Plot of median diameter (Md_ϕ) against distance from vent (a) and against sorting parameter (b) for deposits associated with fallout beyond the cone. "Surge" samples refer to the package of laminated and cross-laminated beds northwest of the cone.

Fig. 10. Scanning electron photomicrograph of ash from the laminated and cross laminated sequence within the fallout deposits ~200-300 m NW of the cone (Column D; Table 2). Note abrasion of some grains.

Fig. 11. Aerial photo of the medial and distal parts of the northeast lava field, illustrating lobate nature of the flow margin. Lines show the eastern edge of the south lava field and the west edge of the northeast lava field (dashed where flow margins are not visible due to coverage by eolian sand). Dotted pattern indicates possible ripply surface ridges (largely obscured by eolian sands) along what might have been a main surface lava channel.

Fig. 12. Photographs of features along margins of the northeast lava field. (a) Down stepping lobes (arrows) representing successive tube-fed breakouts of lava from the toes of lobes, along eastern margin of the lava field. Lowermost lobes are ~1 m high (original height cannot be determined due to partial burial by eolian sand ramps). (b) Stacking of flow units. Dashed lines indicate outer margins of two flow units. The lower unit formed a ~100 m wide, 3-5 m high platform where lava abutted a hill of Miocene ignimbrite. Later lava lobes were emplaced on top of this platform, as shown by the upper flow front near the right side of the photograph. (c) Low-lying flow units on the northern edge of the northeast lava field were partly buried by a combination of violent Strombolian fallout deposits, by sediment accumulation after the lavas temporarily dammed a drainage from the north, and by eolian sands. Arrows point to the tops of flow edges or squeeze-up features from these low-lying units that protrude above the pyroclastic and sedimentary deposits. Edges of flow units

emplaced on top of the low-lying units are clearly visible. Unlike many stacked flow units, the longest of these, in the middle ground of the photograph (edge indicated by dotted line), did not stop inboard of the underlying flow's edge but flowed over it onto the desert floor. The total length of this unit, which has a central ripply channel that feeds four distributary lobes towards its northern (distal) end, is ~140 m.

Fig. 13. Xenolith concentration (volume fraction) plotted against elevation in the Lathrop Wells cone. Values for volcanoes of the Lucero volcanic field (New Mexico; Valentine and Groves, 1996) and the Hopi Buttes field (Arizona; White, 1991) are shown for comparison.

Fig. 14. Aerial photo of Lathrop Wells cone taken in 1987 before major quarrying. Linear features extending both inward and outward from crater rim are erosional rills (especially visible on the southern half of the cone). Dark-colored arcuate features on outer cone slopes are garlands produced by creep of loose scoria deposits. Light colored area on southeast slope of cone is caused by accumulation of eolian sand and silt at a rate that exceeds the rate at which the sediments can infiltrate into the underlying scoria (see also Valentine and Harrington, 2006).

Fig. 15. Cross-section to illustrate evidence for the erosional history of the Lathrop Wells cone. (a) West-east profile of cone through the crater center. Dashed rectangle defines part of profile detailed in (b). (b) Cross section through western crater rim, showing locations of trenches and depositional units (oxidized tephra, black tephra, and crater-filling colluvium) that constrain the degree of erosion of the rim (dashed line extrapolates basal contact of black tephra unit above modern rim).

Fig. 16. Photograph illustrating mechanical weathering of a small lava crag on the northeast lava field. Fragments of the crag are produced by freeze-thaw and thermal spalling of the lava,

especially on the south (sunward) face of the crag (shown in the photograph). Where the clasts accumulate around the crag they begin to stabilize the eolian sediments and evolve towards a desert pavement.

Fig. 17. An interpretation (top to bottom) of the effusive and explosive processes that formed the Lathrop Wells volcano. Earliest (plagioclase phenocryst-bearing) lava flows to the southwest of the developing cone were contemporaneous with Strombolian explosions that ejected mainly coarse, ballistic bombs to form variably welded deposits. Strombolian cone building continued through the development of the remainder of the south lava field, and was counteracted to varying degrees by rafting of material atop the lavas. The south lava field increased in thickness in proximal areas, progressively diverting emerging lavas toward the north. Violent Strombolian activity produced multiple eruption column events and buried the south lava field and the early parts of the northeast lava field. Development of the remainder of the northeast lava field continued after violent Strombolian activity had waned, such that only remnants of ash and fine lapilli are present.

Table 1
Representative compositions* of early and late stage lavas from Lathrop Wells volcano

Sample	LW22FVP	LW61FVP
	Western lobe of south lava field	Late breakout from northeast lava field
Major Elements	wt%	wt%
SiO2	47.43	48.65
TiO2	2.06	1.83
Al2O3	16.60	16.87
Fe2O3	12.15	11.45
MnO	0.18	0.18
MgO	6.13	5.70
CaO	8.40	8.79
Na2O	3.55	3.39
K2O	1.80	1.80
P2O5	1.31	1.17
Total	99.60	99.82
Trace Elements	ppm	ppm
V	184.6	187.6
Cr	106.2	110.3
Co	31.5	29.8
Ni	61.7	46.9
Rb	14.0	19.8
Sr	1555.9	1450.2
Y	23.5	22.6
Zr	381.8	370.5
Ba	1314.8	1375.7
Sc	18.7	19.7
La	92.6	94.1
Ce	184	179
Sm	12.7	12.0
Eu	3.28	3.06
Tb	1.17	1.10
Yb	2.42	2.34
Lu	0.356	0.338
Hf	7.17	7.12
Ta	1.39	1.37
Th	6.05	7.29

Table 2
Coordinates of measured stratigraphic sections of fallout deposits.

Column	Latitude	Longitude
Z	N36° 40' 49.4"	W116° 30' 22.9"
K	N36° 40' 54.8"	W116° 30' 26.0"
X	N36° 41' 28.6"	W116° 30' 49.5"
Y	N36° 41' 31.8"	W116° 30' 54.1"
J	N36° 41' 36.1"	W116° 31' 02.4"
I	N36° 41' 39.2"	W116° 31' 03.1"
D	N36° 41' 42.7"	W116° 30' 53.5"
F	N36° 41' 53.0"	W116° 30' 44.2"
E	N36° 42' 14.0"	W116° 30' 53.9"
B	N36° 42' 44.3"	W116° 30' 55.3"

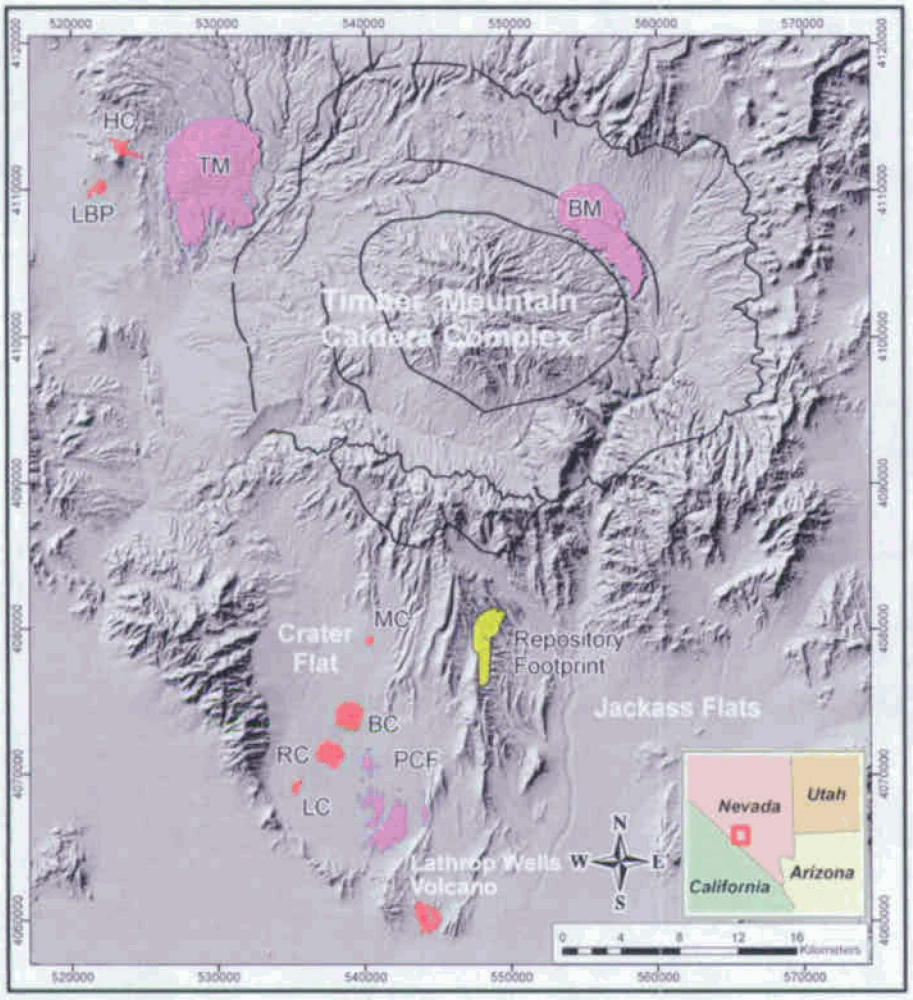
520000
530000
540000
550000
560000
570000
4120000
4110000
4100000
4090000
4080000
4070000
4060000
HC
TM
LBP
BM
Timber Mountain
Caldera Complex
MC
Crater
Flat
Repository
Footprint
Jackass Flats
BC
RC
PCF
LC
Lathrop Wells
Volcano
N
W
E
S
Nevada
Utah
California
Arizona
0
4
8
12
16
Kilometers

Figure 1

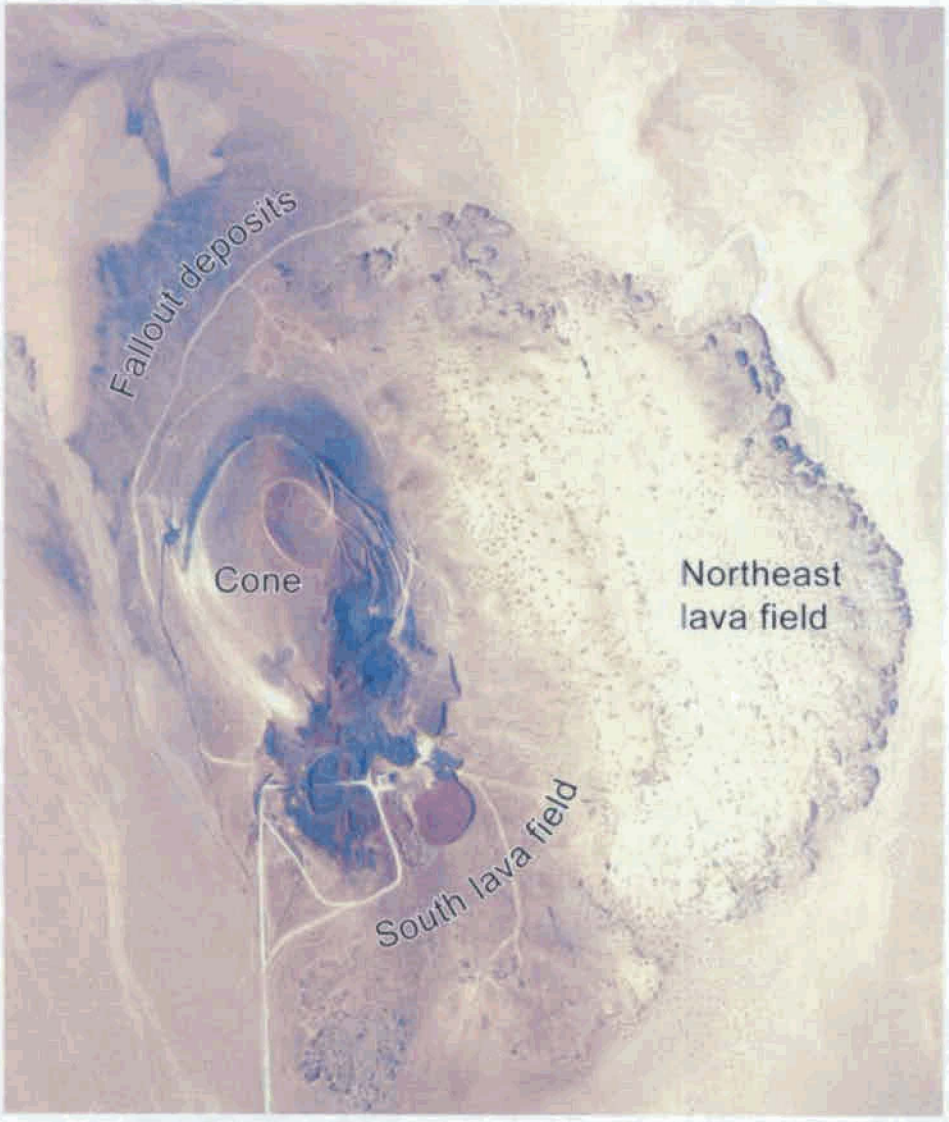
Fallout deposits
Cone
Northeast
lava field
South lava field

Figure 2a

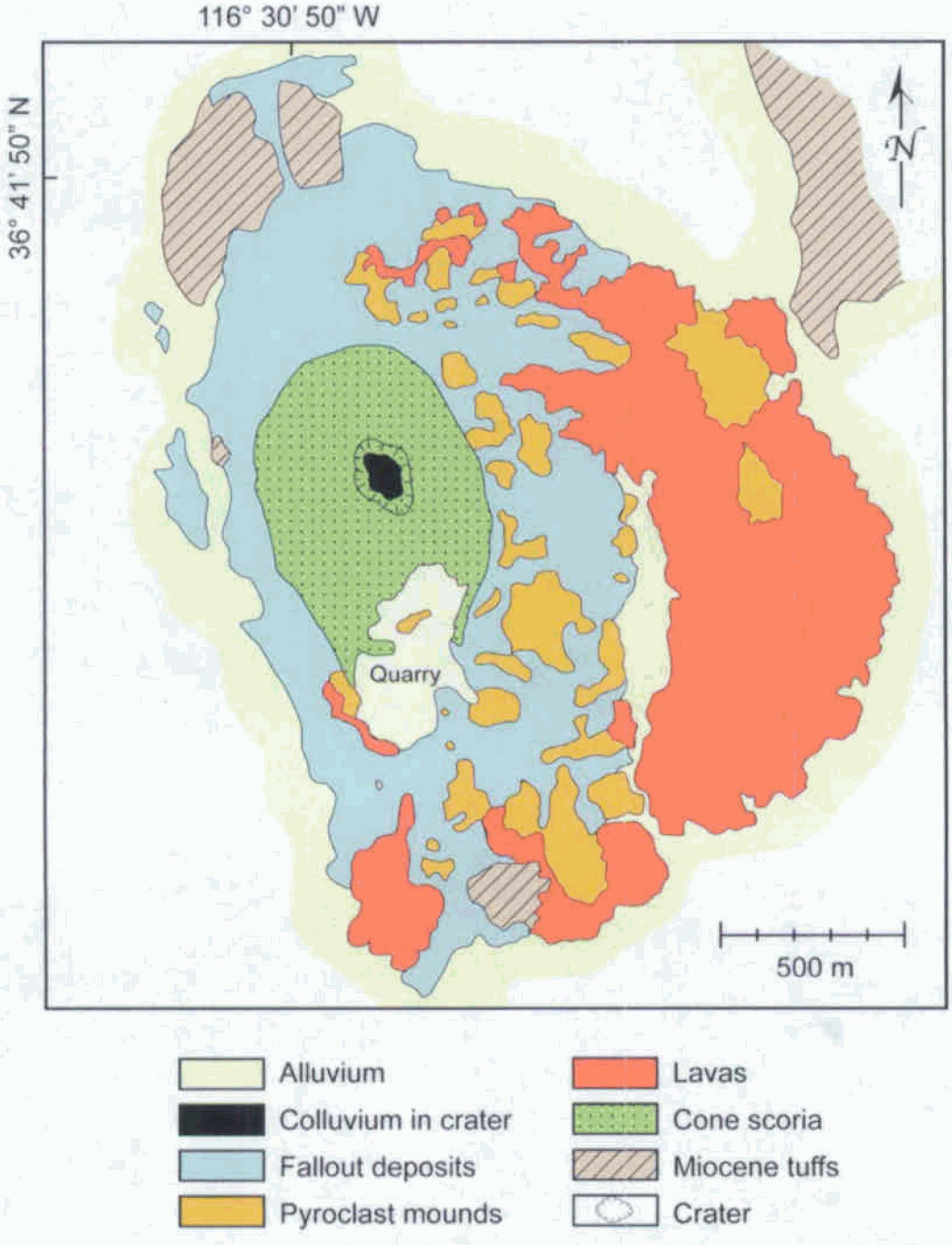
116° 30' 50" W
36° 41' 50" N
N
Quarry
500 m
Alluvium
Colluvium in crater
Fallout deposits
Pyroclast mounds
Lavas
Cone scoria
Miocene tuffs
Crater

Figure 2b

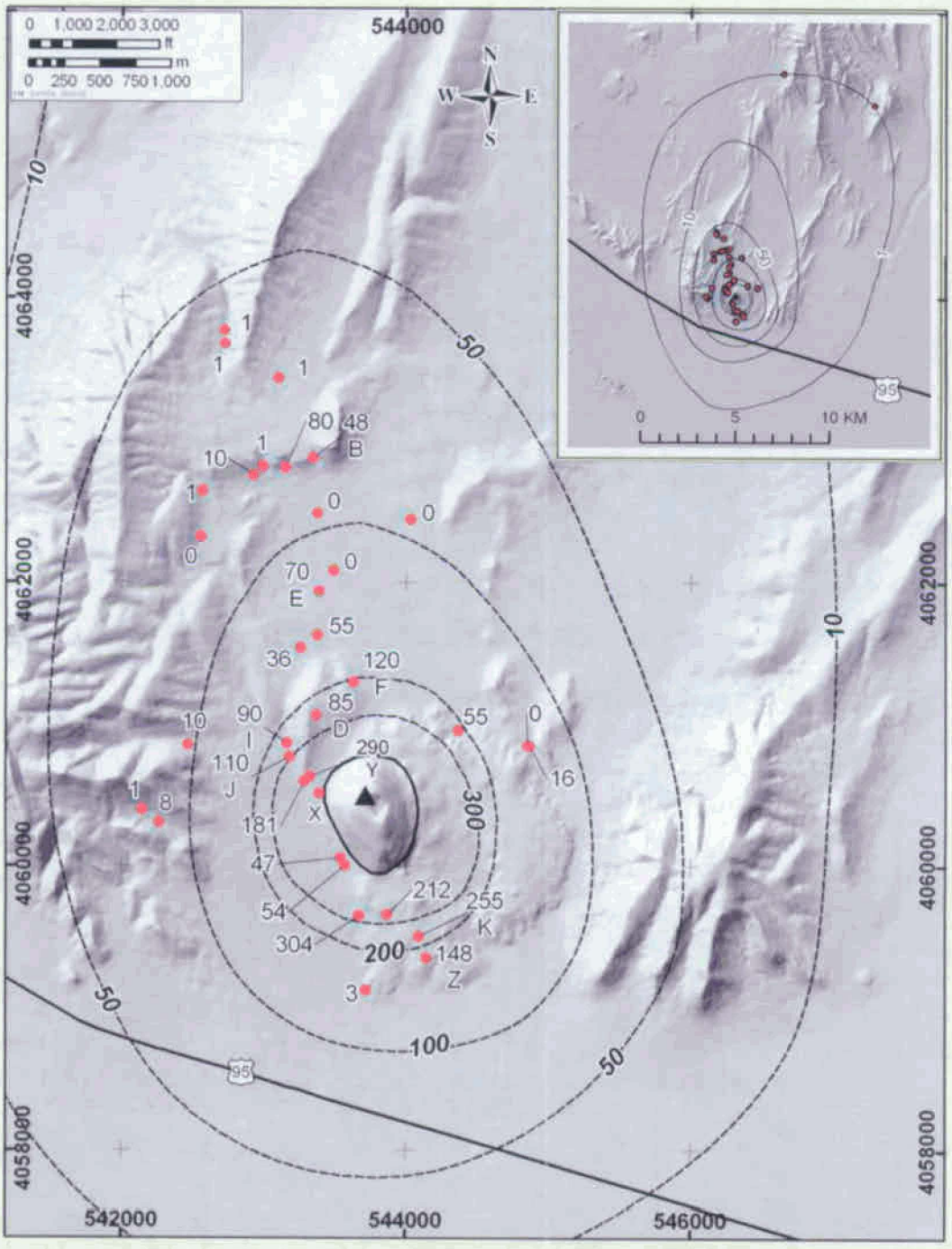
0 1,000 2,000 3,000
ft
m
0 250 500 750 1,000
544000
N
W
E
S
0 5 10 KM
95
4064000
4062000
4060000
4058000
542000
544000
546000
10
50
100
200
300
1
80
48
B
10
0
70
E
55
36
120
F
85
D
90
I
110
J
290
Y
X
181
47
54
304
212
255
K
148
Z
3
16

Figure 2c

Figure 3

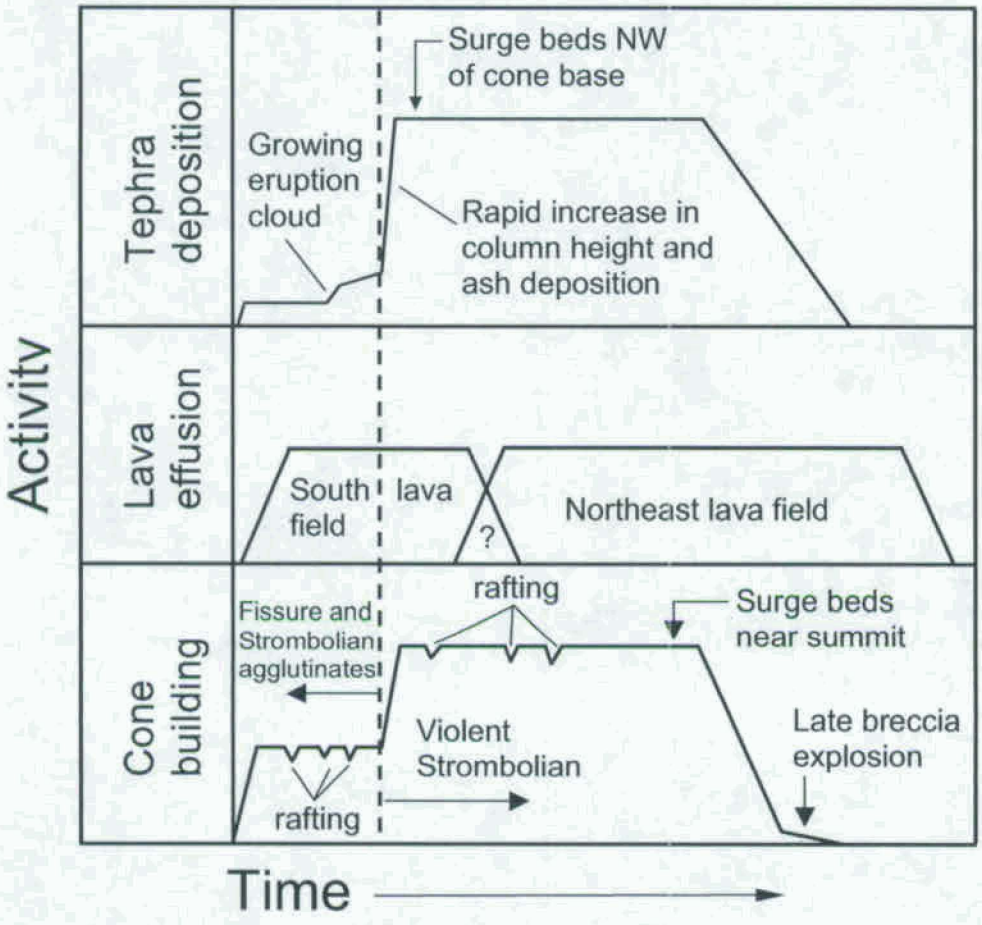
Activity
Tephra deposition
Surge beds NW of cone base
Growing eruption cloud
Rapid increase in column height and ash deposition
Lava effusion
South field lava
?
Northeast lava field
Cone building
Fissure and Strombolian agglutinates
rafting
Surge beds near summit
Violent Strombolian
Late breccia explosion
rafting
Time

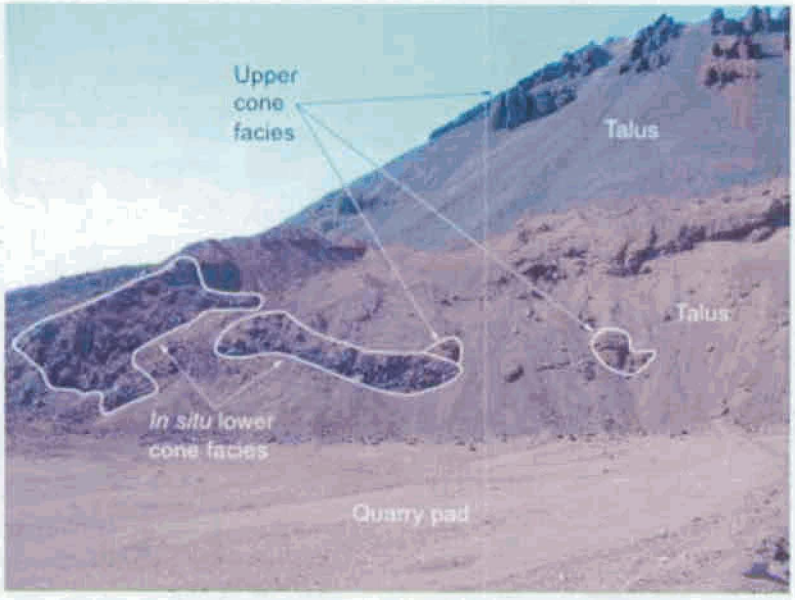
Upper
cone
facies
Talus
Talus
In situ lower
cone facies
Quarry pad

Figure 4

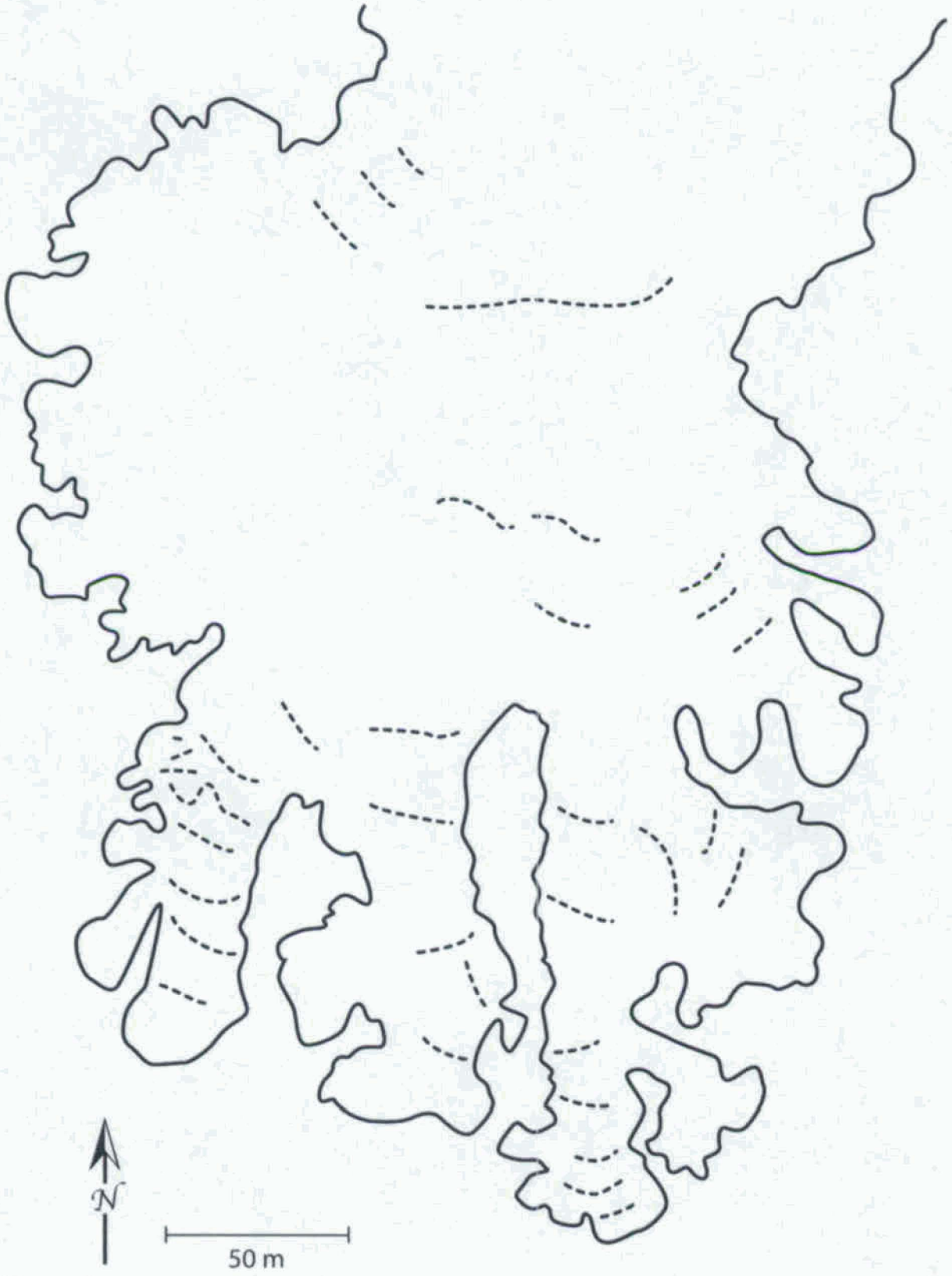

Figure 5

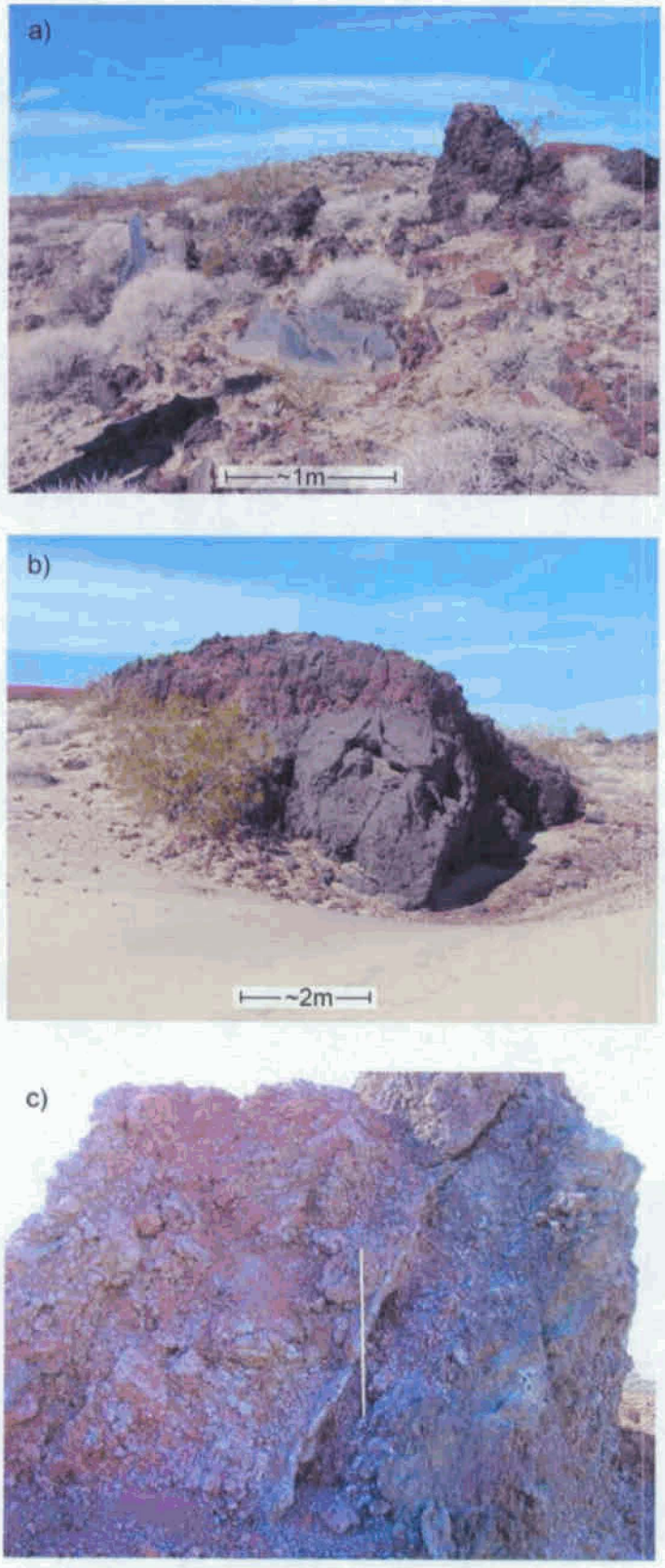

Figure 6

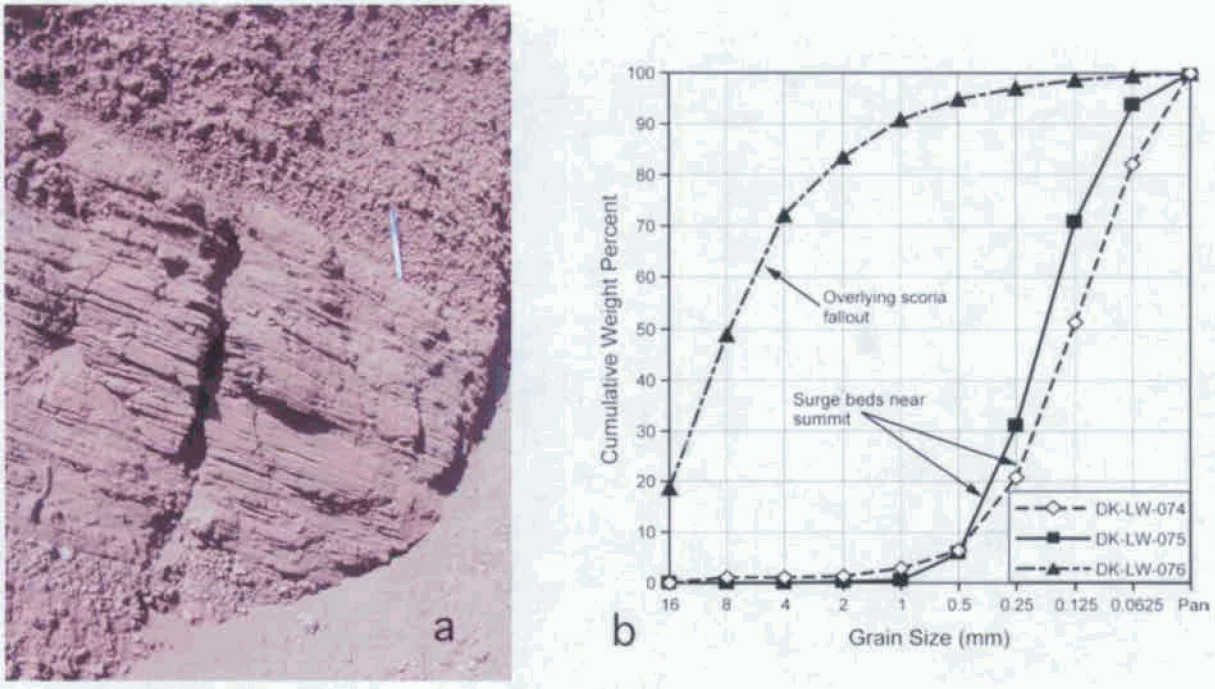
a
b
Cumulative Weight Percent
Grain Size (mm)
Overlying scoria fallout
Surge beds near summit
DK-LW-074
DK-LW-075
DK-LW-076
100
90
80
70
60
50
40
30
20
10
0
16
8
4
2
1
0.5
0.25
0.125
0.0625
Pan

Figure 7

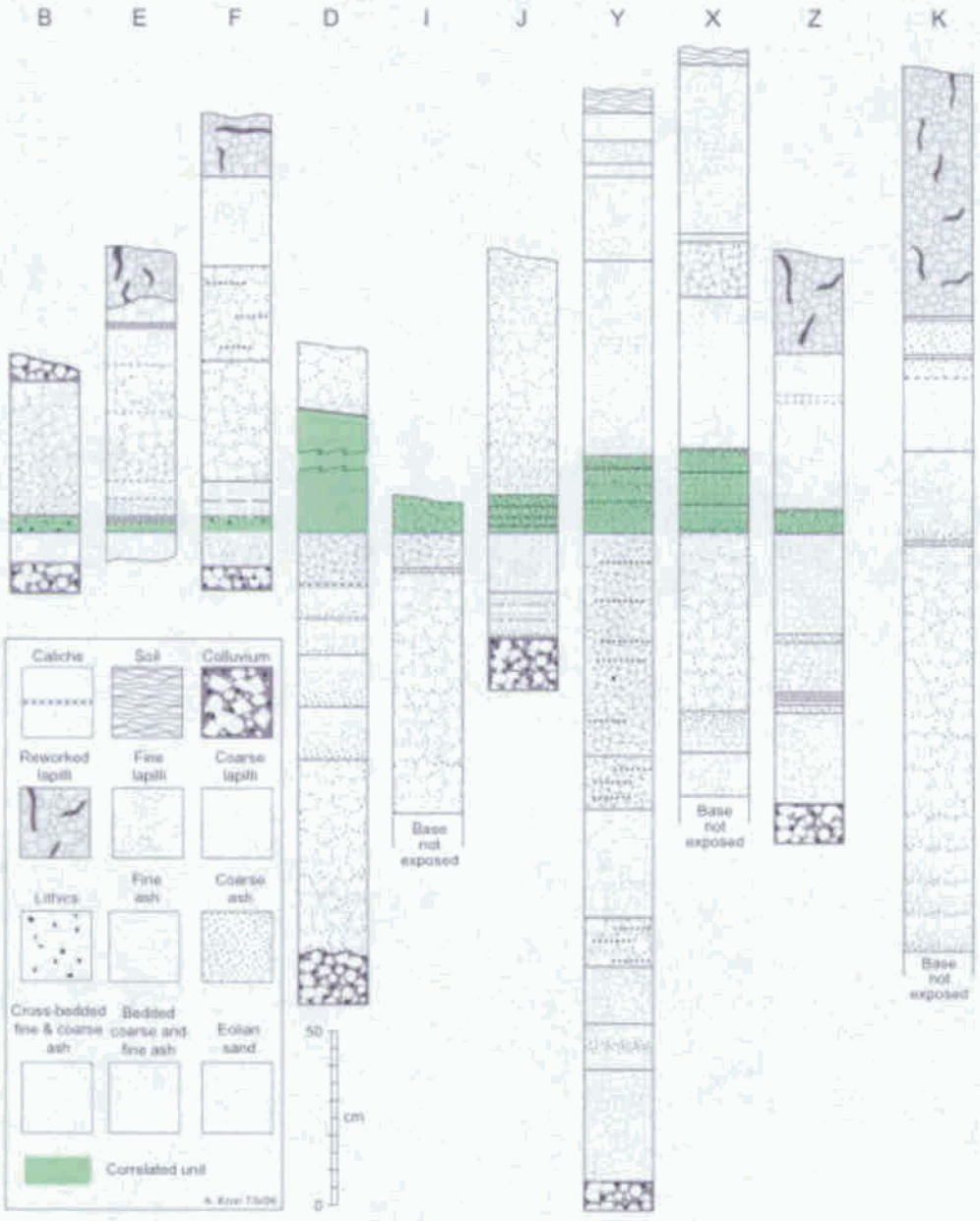
B
E
F
D
I
J
Y
X
Z
K
Caliche
Soil
Colluvium
Reworked lapilli
Fine lapilli
Coarse lapilli
Lithics
Fine ash
Coarse ash
Cross-bedded fine & coarse ash
Bedded coarse and fine ash
Eolian sand
Correlated unit
Base not exposed
Base not exposed
Base not exposed
50
cm
0

Figure 8

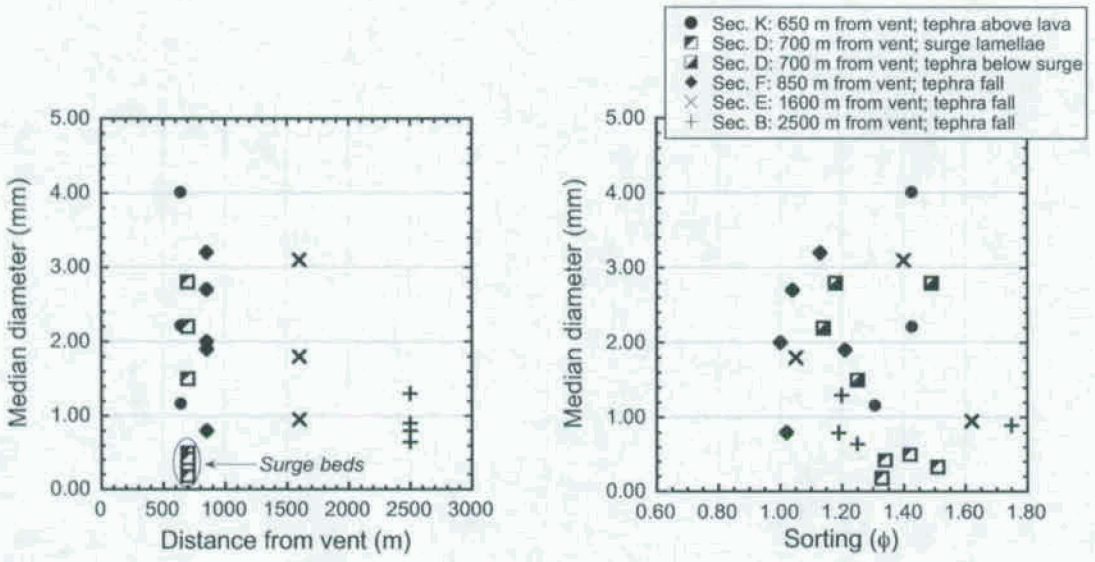
Median diameter (mm)
5.00
4.00
3.00
2.00
1.00
0.00
0
500
1000
1500
2000
2500
3000
Distance from vent (m)
Surge beds
Sec. K: 650 m from vent; tephra above lava
Sec. D: 700 m from vent; surge lamellae
Sec. D: 700 m from vent; tephra below surge
Sec. F: 850 m from vent; tephra fall
Sec. E: 1600 m from vent; tephra fall
Sec. B: 2500 m from vent; tephra fall
Median diameter (mm)
0.60
0.80
1.00
1.20
1.40
1.60
1.80
Sorting (ϕ)

Figure 9

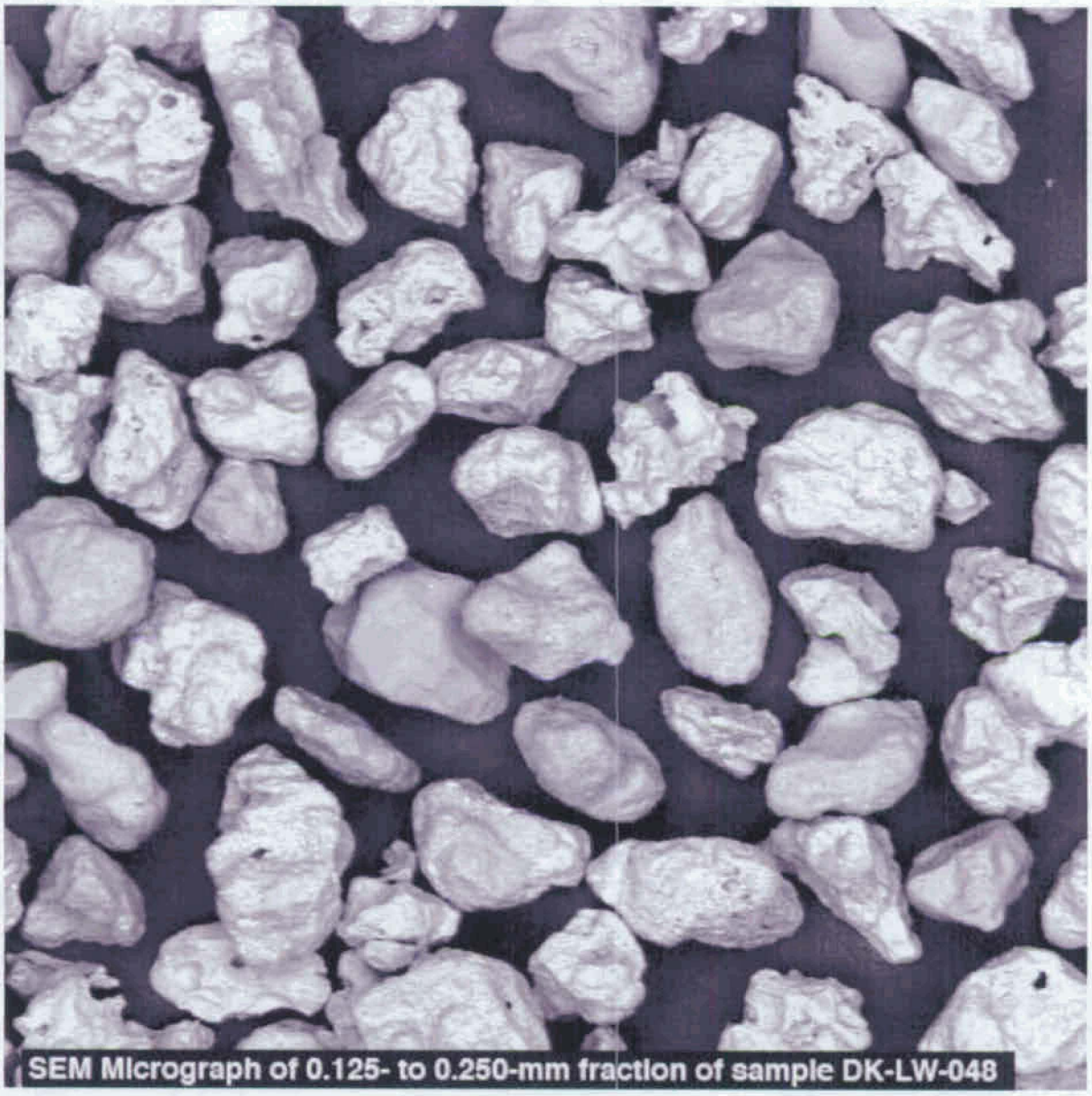
SEM Micrograph of 0.125- to 0.250-mm fraction of sample DK-LW-048

Figure 10

Figure 11

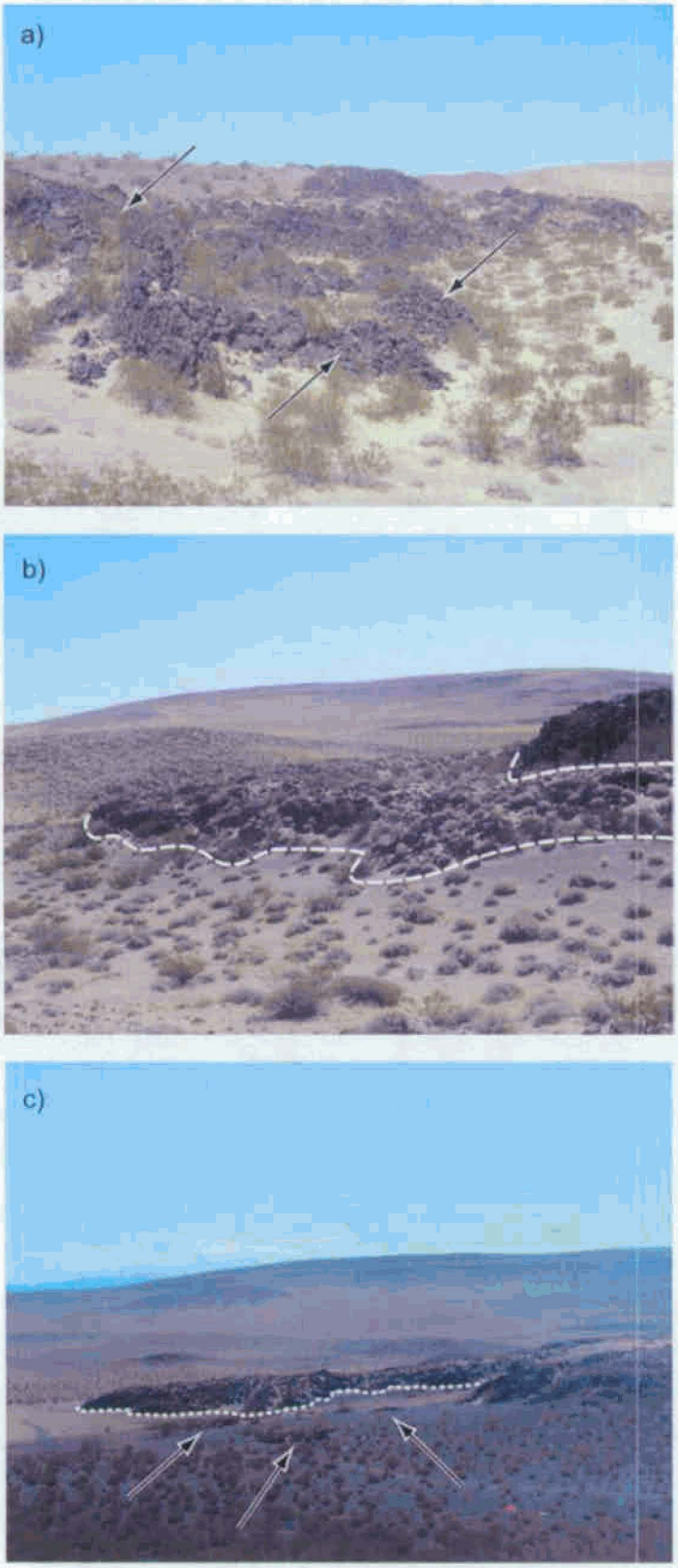

Figure 12

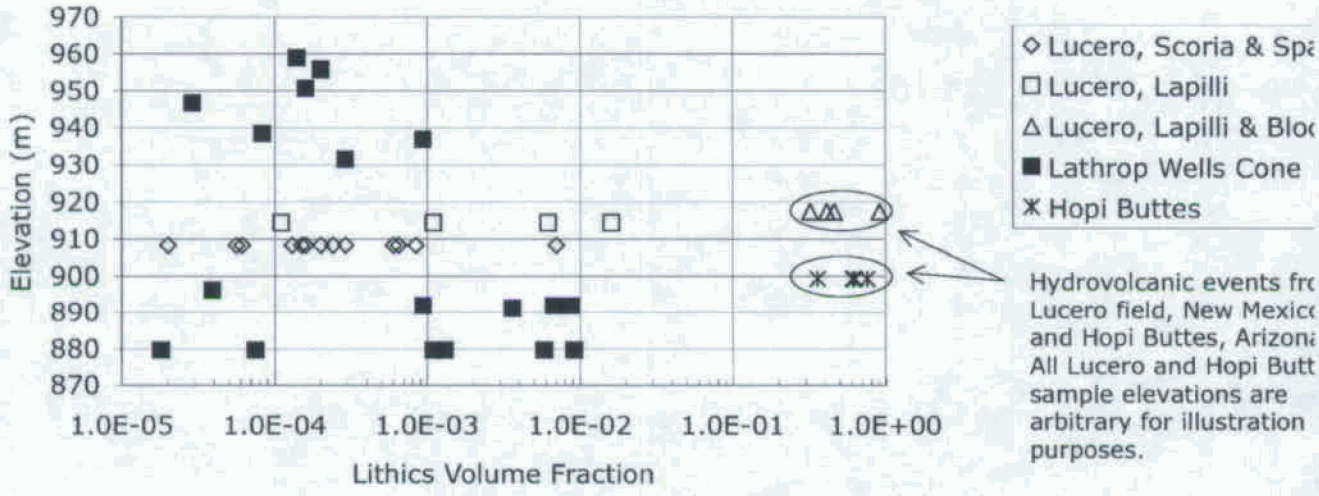
970
960
950
940
930
920
910
900
890
880
870
Elevation (m)
1.0E-05
1.0E-04
1.0E-03
1.0E-02
1.0E-01
1.0E+00
Lithics Volume Fraction
◇ Lucero, Scoria & Spa
□ Lucero, Lapilli
△ Lucero, Lapilli & Bloc
■ Lathrop Wells Cone
✳ Hopi Buttes
Hydrovolcanic events fr
Lucero field, New Mexic
and Hopi Buttes, Arizon
All Lucero and Hopi Butt
sample elevations are
arbitrary for illustration
purposes.

Figure 13

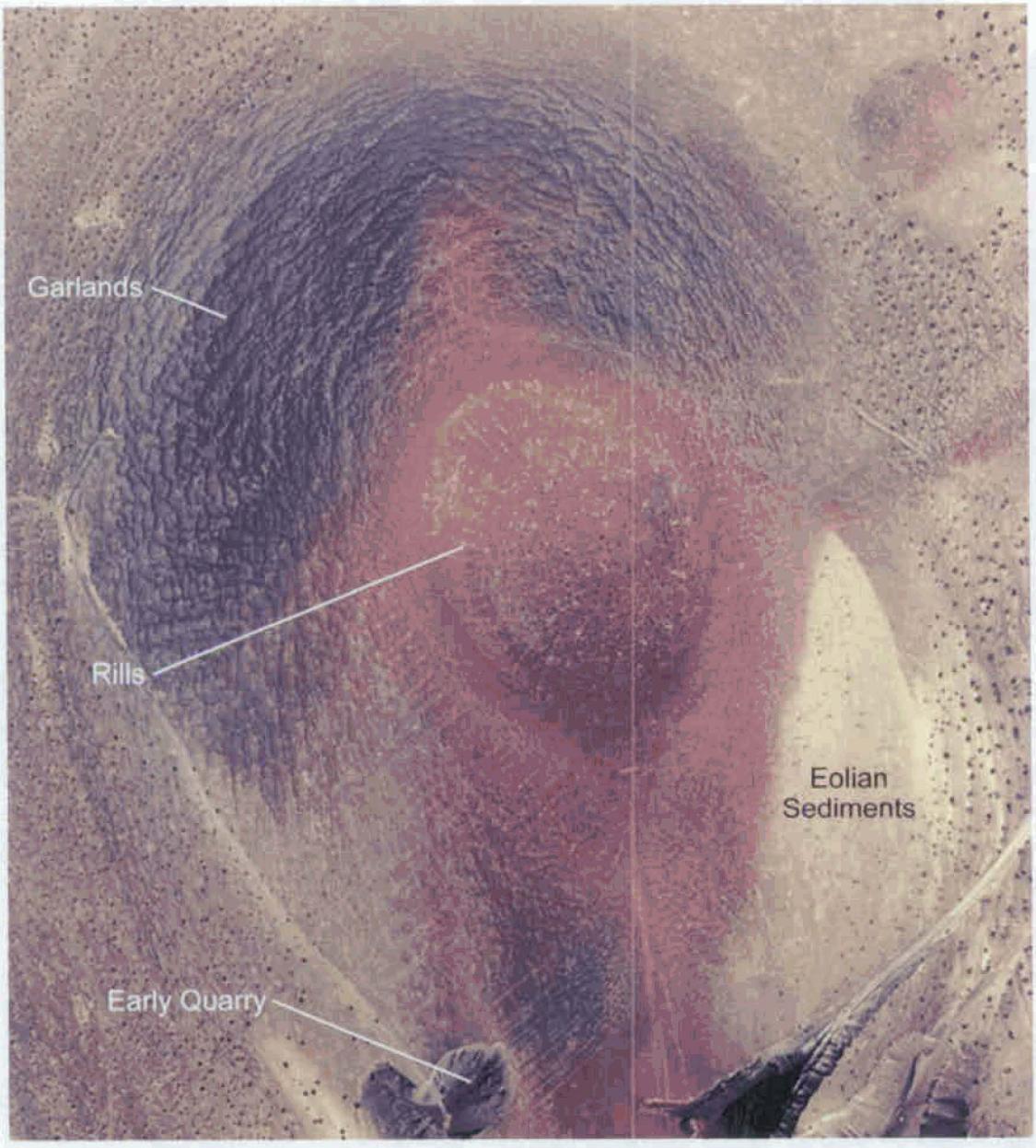

Figure 14

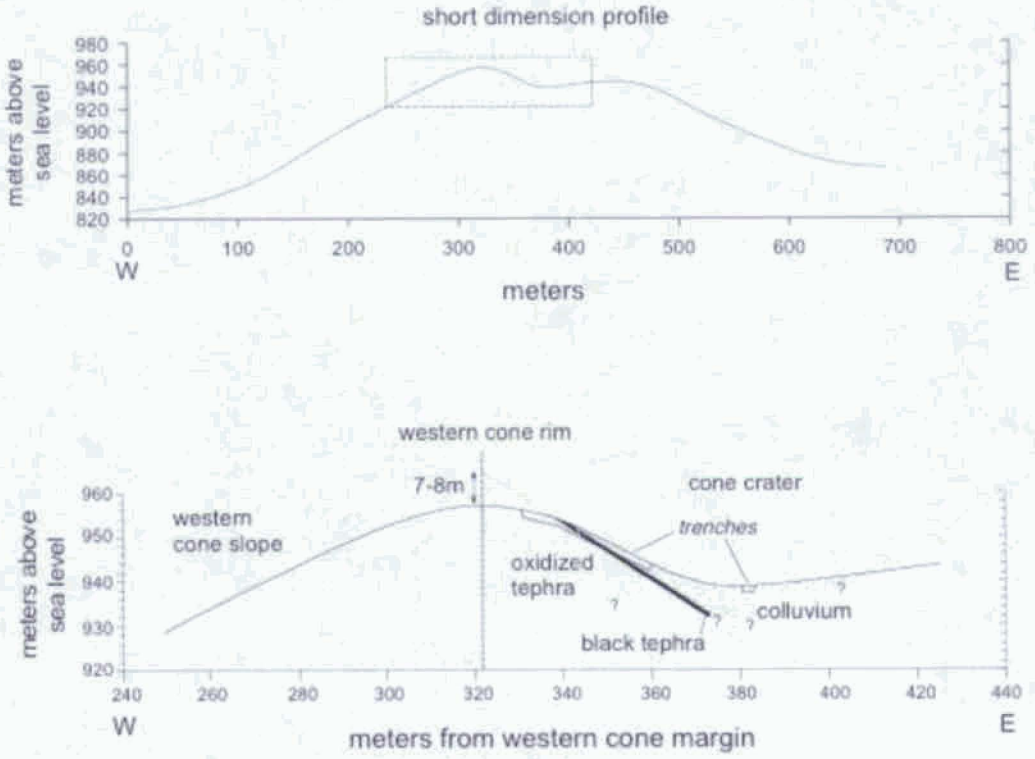
short dimension profile
meters above sea level
980
960
940
920
900
880
860
840
820
0
100
200
300
400
500
600
700
800
W
E
meters
western cone rim
7-8m
cone crater
western cone slope
trenches
oxidized tephra
colluvium
black tephra
meters above sea level
960
950
940
930
920
240
260
280
300
320
340
360
380
400
420
440
W
E
meters from western cone margin

Figure 15

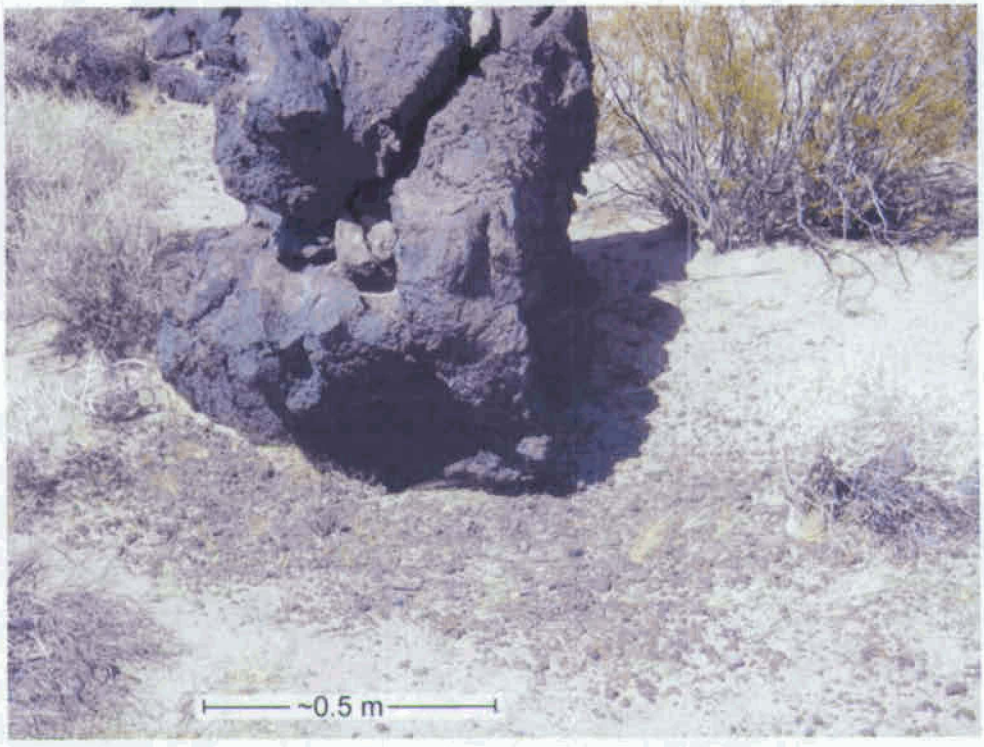

Figure 16

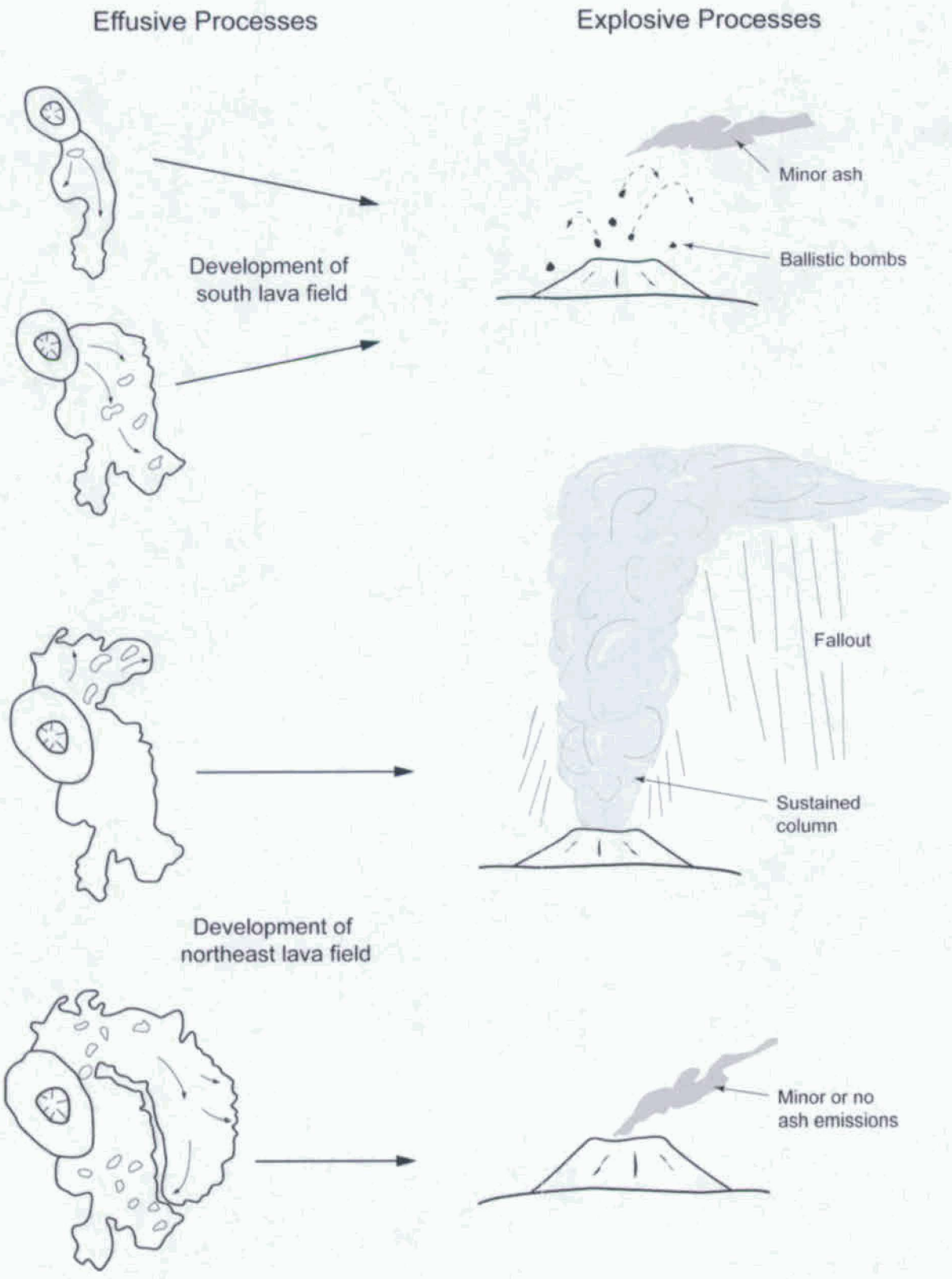
Effusive Processes
Explosive Processes
Minor ash
Ballistic bombs
Development of
south lava field
Fallout
Sustained
column
Development of
northeast lava field
Minor or no
ash emissions

Figure 17